NASA TECHNICAL MEMORANDUM

NASA TM X-1841

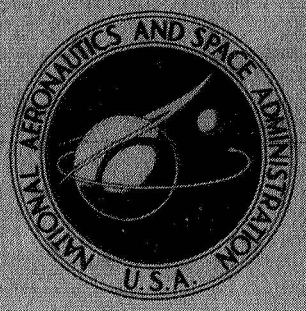

NASA TM X-1841

AN EVALUATION TEST OF A FULL-SCALE REPLICA OF THE RAM-CA FLIGHT HEAT SHIELD IN A ROCKET-ENGINE EXHAUST

by Kenneth Sutton, Ernest V. Zoby, and David H. Butler

Langley Research Center
Langley Station, Hampton, Va.

NATIONAL AERONAUTICS AND SPACE ADMINISTRATION • WASHINGTON, D. C. • JULY 1969

1. Report No. NASA TM X-1841	2. Government Accession No.	3. Recipient's Catalog No.
4. Title and Subtitle AN EVALUATION TEST OF A FULL-SCALE REPLICA OF THE RAM-CA FLIGHT HEAT SHIELD IN A ROCKET-ENGINE EXHAUST		5. Report Date July 1969 6. Performing Organization Code
7. Author(s) Kenneth Sutton, Ernest V. Zoby, and David H. Butler		8. Performing Organization Report No. L-6164
9. Performing Organization Name and Address NASA Langley Research Center Langley Station Hampton, Va. 23365		10. Work Unit No. 124-08-03-05-23 11. Contract or Grant No. 13. Type of Report and Period Covered Technical Memorandum
12. Sponsoring Agency Name and Address National Aeronautics and Space Administration Washington, D.C. 20546		14. Sponsoring Agency Code
15. Supplementary Notes		

16. Abstract

An evaluation test of the RAM-CA heat shield was conducted in a rocket engine exhaust at the General Electric Malta Test Station using a full-scale replica of the flight heat shield. The primary purpose of the test was to study some possible problems that would affect the heat-shield design and that could not be completely simulated on small models in the materials research test facilities at the Langley Research Center. Of special concern in the present evaluation were the effects on the heat-shield performance of the hole patterns in the phenolic-carbon material at the nose region and of the junction between the phenolic-carbon material and teflon used along the afterbody. The present test evaluation did not show any problems that would disqualify the RAM-CA heat-shield design for flight application.

17. Key Words Suggested by Author(s) Heat-shield design Ablation and heating	18. Distribution Statement Unclassified – Unlimited		
19. Security Classif. (of this report) Unclassified	20. Security Classif. (of this page) Unclassified	21. No. of Pages 47	22. Price* $3.00

*For sale by the Clearinghouse for Federal Scientific and Technical Information
Springfield, Virginia 22151

AN EVALUATION TEST OF A FULL-SCALE REPLICA OF THE RAM-CA FLIGHT HEAT SHIELD IN A ROCKET-ENGINE EXHAUST

By Kenneth Sutton, Ernest V. Zoby,
and David H. Butler
Langley Research Center

SUMMARY

An evaluation test of the RAM-CA heat shield was conducted in a rocket engine exhaust at the General Electric Malta Test Station using a full-scale replica of the flight heat shield. The primary purpose of the test was to study some possible problems that would affect the heat-shield design and that could not be completely simulated on small models in the materials research test facilities at the Langley Research Center. Of special concern in the present evaluation were the effects on the heat-shield performance of the hole patterns in the phenolic-carbon material at the nose region and of the junction between the phenolic-carbon material and teflon used along the afterbody. The present test evaluation did not show any problems that would disqualify the RAM-CA heat-shield design for flight application.

INTRODUCTION

Project RAM (Radio Attenuation Measurement) at the Langley Research Center is concerned with the entry communication problem and makes extensive use of flight vehicles to obtain experimental data. (See refs. 1 and 2.) The purpose of the RAM-CA flight experiment is to study the effects of injecting water into the flow field to alleviate the blackout of radio communications. The RAM-CA reentry package has a hemispherical nose with a conical afterbody. The heat shield in the nose region and the front part of the afterbody is Narmco 4028 (a phenolic resin-carbon fiber composite). Teflon is used as the heat-shield material along the remaining portion of the afterbody. There are hole patterns in the Narmco 4028 at the stagnation region and at two locations along the afterbody for the injection of water during the flight experiment.

An experimental ground study was conducted to verify the adequacy of the carbon-phenolic heat shield for flight. These tests were conducted using small models in the materials research test facilities at the Langley Research Center. However, there were several unique features inherent in the RAM-CA heat-shield design that could not be

completely studied on the small models in Langley's high-enthalpy test facilities. It was considered necessary to test a full-scale model of the heat-shield nose section to evaluate qualitatively the effects of some possible problems on the ablation performance of the heat-shield design when exposed to a high-temperature flow field. The possible sources of problems are as follows:

(1) Hole pattern at stagnation region

(2) Hole patterns at side walls

(3) Dissimilar material ablation at Narmco-teflon junction

(4) Teflon plugs (3) used to cover mechanical connectors of inner structure

(5) Mechanical char removal, especially side wall

(6) Overall bonding and assembly

The ablation test model was a full-scale replica of the first 18 inches (0.46 meter) in length of the RAM-CA flight heat shield. A calibration model which had both pressure and heating-rate sensors was also tested in order to define the present test environment. The tests were conducted at the General Electric Malta test station in August 1966 under contract NAS1-6643. A reentry test facility the test environment of which is the exhaust of an ethyl alcohol—liquid oxygen rocket engine was used for the tests. The purpose of this paper is to present the evaluation of the test results.

SYMBOLS

The units used for the physical quantities defined in this paper are given both in the U.S. Customary and in the International System of Units (SI). (See ref. 3.)

c	specific heat of calorimeter material, Btu/lbm-^{o}F (J/kg-^{o}K)
K_O	effective oxygen mass fraction for char removal
L	thickness of calorimeter, ft (m)
M_O	total oxygen mass flux, lbm/ft^2 (kg/m^2)
$\dot{m}_O$	oxygen mass flux, lbm/ft^2-sec (kg/m^2-s)
p	pressure, atmospheres
Q	total cold-wall heating, Btu/ft^2 (J/m^2)

$\dot{q}$ cold-wall heating rate, Btu/ft^2-sec (W/m^2)

r initial model nose radius (see tables I and III), in. (m)

s distance along initial model surface from stagnation point (see tables I and III), in. (m)

T temperature, ^{o}F or ^{o}R (^{o}K)

t time, sec (s)

V velocity, ft/sec (m/s)

ρ density of calorimeter material, lbm/ft^3 (kg/m^3)

ϕ angle (see tables I and III), deg

Subscripts:

l local condition

s stagnation point

T total condition

1 condition upstream of shock wave

2 condition downstream of shock wave

TEST OBJECTIVES

There were several possible problems with the RAM-CA flight heat shield which could not be completely evaluated on small models in the materials research facilities at the Langley Research Center. The test objectives of the present study were to evaluate the effects of the possible problems on the ablation performance of the heat-shield design and to serve as a final qualification of the flight heat shield.

The ability of holes to maintain their integrity in Narmco 4028 when exposed to a high-temperature flow field was studied on small-scale models, but the complete hole patterns could not be simulated in the small models. The severity of enlargements of the

individual holes, if any, and whether this enlargement would cause interconnection of the holes within a pattern was to be evaluated in the present test. This evaluation was to be conducted for the hole pattern at the stagnation region and the hole patterns at the side wall of the heat shield.

The analysis during the heat-shield design showed that a rearward-facing step would be formed at the Narmco-teflon junction because of the ablation of dissimilar materials. The effect of this step formation on the material ablation in this area needed to be investigated experimentally. The effect on the teflon was considered to be the most important since it is located on the downstream side of the step formation.

Mechanical char removal in addition to oxidation has been observed to occur for Narmco 4028 in the nose region of small models and was accounted for in the final heat-shield design. An evaluation still needed to be made of the occurrence of mechanical char removal on a large model and the effect of the mechanical char removal on the stability of the hole patterns. Mechanical char removal of the Narmco 4028 was not observed to occur along the side wall of the small models. However, mechanical char removal has been observed for similar phenolic-carbon materials on large hemispherical-conical models as discussed in the section "Ablation Model Results." The determination of mechanical char removal along the side wall of the RAM-CA heat shield and the effect on the side-wall hole patterns were especially important in the present test.

The ability of the overall bonding and assembly techniques to keep the heat shield intact also needed to be investigated. This type of investigation can only be satisfactorily conducted on a full-scale model. Teflon plugs are located in the teflon heat shield to protect access holes to mechanical connectors of the inner structure from the thermal environment. An evaluation was necessary to determine whether the seam between the teflon plug and the main teflon heat shield would cause any unusual ablation of the teflon. The ability of the teflon plugs to remain within the access holes also needed to be evaluated.

The present test also allowed for an observation of the possible occurrence of any disqualifying phenomena which had not previously been anticipated in the RAM-CA heat-shield design.

TEST FACILITY

The tests were conducted in the reentry test facility No. 4 of the Malta Test Station which is operated by the General Electric Company. The test environment of this facility is the exhaust of the combustion gases from an ethyl alcohol—liquid oxygen rocket engine with a 15-inch-diameter (0.38-meter) exit. The free-stream Mach number is

approximately 3. The rocket engine is mounted in a vertical position and fires downward. A photograph showing the nozzle exit and model position is shown in figure 1.

The model is held stationary and the rocket engine is swung into position over the model during the test. A water-cooled model holder was used and positioned before the test for correct alinement of the model with the nozzle center line and distance from the nozzle exit. The Malta Test Station provided instrumentation readout from the model, camera coverage of the model, and continual recordings of the rocket engine performance during a test.

DESCRIPTION OF MODELS

Two models were tested during this study. The primary model was a full-scale replica of the first 18 inches (0.46 meter) of the RAM-CA flight heat shield. The heat shield of this test model was thinner than that of the final flight vehicle. The final flight heat shield was made thicker because of the results obtained from the tests on the small-scale models. The present test model was constructed but not tested before the decision was made to increase the thickness of the actual flight heat shield. However, the essential features of the heat shield were duplicated on this ablation test model. The second model was a calibration model of the same shape and size as the ablation model and had sensors to measure heating rate and pressure distributions. A description of each of the models follows.

Ablation Model

The ablation model was a full-scale replica of the front portion of the RAM-CA flight heat shield. The model had a 6-inch radius (0.152 meter) hemispherical nose and a 9^{o} conical afterbody. The maximum diameter of a model which can be tested in the facility is 16 inches (0.406 meter). Therefore the test model was truncated to a length of $17\frac{3}{4}$ inches (0.451 meter) as compared with a length of 51 inches (1.29 meters) for the flight model. A drawing of the model is shown in figure 2. A sketch of the coordinate system used in this report and the location of essential features are given in table I. All surface locations (s/r) used in this report are based on the initial model shape. Photographs of a side and top view of the model before testing are shown in figure 3.

The ablation material on the hemisphere and along the afterbody to an s/r of 2.12 is Narmco 4028. This material is a charring ablator composed of 50 percent by weight of phenolic resin and 50 percent of 0.25-inch-long (0.63 cm) carbon fibers. The density of the virgin material is 87 lbm/ft^3 (1392 kg/m^3). The material aft of $s/r = 2.12$ is teflon, a subliming ablator, with a density of 137 lbm/ft^3 (2192 kg/m^3). The thickness of

Narmco 4028 for the present test model was based on the initial flight design. (See table II.) As mentioned previously, the final flight heat shield was thicker than that of the present test model. In the final design of the flight heat shield, the thickness of Narmco 4028 is 1.16 inches (2.95 cm) at the stagnation point and 0.60 inch (1.52 cm) at the Narmco-teflon junction. The thickness of teflon on the test model varied from 0.40 inch (1.02 cm) at $s/r = 2.12$ to 0.33 inch (0.84 cm) at the base. A sublayer of teflon, 0.10 inch (0.25 cm) thick by 1.8 inches (4.51 cm) long, was located under the main teflon layer at the Narmco-teflon junction. This sublayer of teflon is for added protection against the possibility of severe ablation of the teflon at this location caused by the formation of the rearward-facing step at the Narmco-teflon junction. A bond line of high-temperature epoxy adhesive is between the two layers of teflon.

The substructure of the model is made in two sections and joined by three mechanical connectors. The section under the Narmco 4028 material is constructed of stainless steel. A modified epoxy adhesive is used for the bond between the Narmco 4028 and the stainless steel. Aluminum is used for the substructure under the teflon with a high-temperature epoxy adhesive as the bonding agent. The access holes to the mechanical connectors of the substructure were protected from the thermal environment with teflon plugs located in the teflon heat shield. The method of installation of the teflon plugs requires no bonding agent in the seam between the teflon plugs and the main teflon heat shield. The method of fabrication and assembly of the present test model is the same as that used for the flight vehicle.

The stagnation-area hole pattern and the two side-wall hole patterns (180° apart) used on the RAM-CA flight for water injection during the experiment were duplicated on the ablation model. These hole patterns are shown in figures 3 and 4. The holes at the stagnation region are 0.06 inch (0.15 cm) in diameter and the side-wall holes are 0.10 inch (0.25 cm) in diameter. In the flight vehicle the inflow of air through these holes is stopped by the valving system for the water. In the present test model the holes were not drilled completely through the heat shield and therefore the gas flow could not enter the model.

Twenty-five thermocouples were connected to the model to monitor the temperature rise at the back of the heat shield. The location of these thermocouples is given in table I. Seventeen of the thermocouples (thermocouples 1 to 17) were located in the bond line under the Narmco 4028 material. The remaining eight thermocouples (thermocouples 18 to 25) were used to measure the temperature behind the teflon at the sublayer location and were attached to the inside of the inner shell. All thermocouples were constructed of 30-gage chromel-alumel wire. The thermocouples in this model do not duplicate the location of thermocouples in the flight model.

Pressure measurement taps were in the Narmco 4028 heat shield at six locations along the element $\phi = 180^{o}$. The s/r locations for the pressure taps are given in table I. The pressure taps were 0.06 inch (0.15 cm) in diameter, and stainless-steel tubing of 0.090 inch (0.23 cm) outside diameter and 0.060 inch (0.15 cm) inside diameter was used for the connections to electrical strain gages. The pressure tap in the stagnation region ($s/r = 0.05$) was one of the holes used to simulate the water injection holes. There are no pressure taps in the flight model. The pressure distribution around the test model was measured in order to check on the repeatability of the test environment by comparing the pressure results between the ablation test model and the calibration model.

Calibration Model

A drawing of the calibration model is shown in figure 5. The model in the photograph of figure 1 is the calibration model. This model had heating-rate sensors and pressure taps located in a thick-wall, mild-steel shell. The thickness of the shell was 0.75 inch (1.91 cm) at the stagnation region and 0.375 inch (1.45 cm) along the side wall.

The heating-rate measurements were made by using sensors mounted in the model at eight locations. The location of these sensors is shown in table III. The sensors were of the thin-wall slope-type calorimeter. The heating rate was measured by using the temperature-rise rate of a 30-gage chromel-alumel thermocouple attached to the back side of the thin wall of the sensor and the following equation:

$$\dot{q} = \rho c L \frac{dT}{dt}$$

The sensor was made of "K" monel and had a wall thickness of 0.062 inch (0.157 cm) and a diameter of 0.625 inch (1.587 cm). There was a slight air gap between the sensor and the main body of the model to reduce conduction losses.

The pressure measurements were made by the use of pressure taps drilled in the main body of the model. The pressure connections from the model to electrical strain gages were of stainless-steel tubing with 0.090 inch (0.23 cm) outside diameter and 0.060 inch (0.15 cm) inside diameter. There were seven locations of pressure measurements and these locations are given in table III. The pressure taps were located along an element 90^{o} from the heating-rate sensors.

TEST PROCEDURE AND DATA ACQUISITION

Only one model can be tested during the rocket firing. Therefore, the ablation model and the calibration model were tested at separate firings. The model was positioned to be in the center of the nozzle exit and $4\frac{1}{16}$ inches (10.32 cm) from the exit

plane. As previously stated, the model is stationary in a vertical position and the rocket engine is swung over the model after the rocket has obtained an equilibrium flow condition. The time from the ignition of the rocket engine until it is gimbaled fully over the model is 8.5 seconds. However, the time of travel of the rocket engine over the model to center position is only 0.1 second. In this paper, time zero is taken as the time when the rocket engine is fully over the model.

In this facility the sequence of events is controlled by an automatic programer. The end of the test can be set for a predetermined time or the rocket engine can be stopped manually. As a standard procedure at this facility, a thermocouple is inserted in the interior of the model, and if there is a burnthrough of the model, this thermocouple will indicate a rapid temperature rise and the rocket engine will be stopped manually.

The millivolt outputs from the thermocouples on the models, except for three, were recorded on an oscillograph recorder. The temperatures from three of the thermocouples (thermocouples 5, 7, and 20) on the ablation model were recorded on direct-readout strip-chart recorders for monitoring during the test. The outputs from the electrical strain gages for pressure measurements were also recorded on an oscillograph recorder. Calibrations of the oscillograph recorders were made prior to the tests with the models in position for the tests to correlate the oscillograph readings to temperature and pressure. Also, resistivity checks were made of the thermocouples to insure continuity of the connections. Both a two-color pyrometer and a photographic pyrometer were used to measure the surface temperature of the ablation model. The two-color pyrometer averaged the temperature over an area of $1\frac{1}{2}$ inches (2.86 cm) in diameter at the location of $s/r = 0.95$. The photographic pyrometer (see ref. 4) takes a 35-millimeter motion picture of the model and for this particular test most of the Narmco 4028 heat shield was in view. In the readout of the photographic pyrometer data, the temperature was an average over an area 0.10 inch (0.25 cm) in diameter at a particular location. Both instruments were viewing along an element ϕ of approximately 120°.

The test time for the calibration model was preset for 2 seconds. The test of the ablation model was to be manually stopped when any one of the three monitored thermocouples (thermocouple 5, 7, or 20) had a temperature rise of approximately 350 F° (195 K°). A temperature rise of 350 F° (195 K°) was the design criterion for flight. There was a system designed to flow nitrogen over the Narmco 4028 after the end of the test to cool the surface and to reduce the reaction of the hot surface with the atmosphere.

The surfaces of the models could not be observed during the tests because of the intensity of the hot combustion gases. However, there was motion-picture coverage of the tests with low-speed and high-speed cameras (60 to 600 frames per second).

ANALYSIS OF TEST ENVIRONMENT

The reentry test facility used at Malta does not have a well-defined test environment. Although numerous full-scale ablation models have been tested in this facility, there have been only a limited number of calibration models tested to define the flow field. Because of the limited amount of stream test data which are available, it was necessary to test a calibration model in order to have an evaluation of the test environment for the RAM-CA ablation model.

The rocket firing data and the good comparison between the pressure distributions (discussed later) indicate that the test environment was the same for both tests. Also, the motion-picture films of the tests showed the flow over the models to be similar. The rocket-engine-firing data for the tests are contained in table IV.

The motion-picture films of the tests showed a stream interference on the models. This interference on the ablation model is shown in figure 6. The flow separated from the model at the location of the interference. The same type of interference also occurred on the calibration model at the same place. However, the position of this stream interference was such that it did not affect the test objectives. The effect of the interference on the lower part of the teflon is discussed subsequently. An evaluation of the test data indicates that this interference is an anomaly of the present test environment and it is not expected to occur in flight.

The results of the pressure measurements for the calibration model and the ablation model are given in table V and are shown in figure 7. The data for the ablation model are for the same time (t = 0.7 sec) as those for the calibration model and before there was sufficient mass loss to have a significant effect on the shape of the ablation model. As shown by the data, there is good agreement between the two models. However, the measured pressure distribution is different from that expected on a hemisphere. Because of the construction of the models, a pressure tap could not be placed at the stagnation point. Extrapolation of the measured data based on a Newtonian type of distribution gives a stagnation pressure on the models of 13.0 atmospheres.

The results of the heating-rate measurement for the calibration model are given in table VI and are shown in figure 8. The calculated results shown in figure 8 are discussed later. There are no data for the stagnation point because of a malfunction of the thermocouple on the stagnation-point sensor. Extrapolation of the remaining data gives a value of 1200 Btu/ft^2-sec (13.60 MW/m^2) for the stagnation-point heating rate. All heating-rate data are for a cold wall (100° F or 311° K).

Calculations were made of the heating rates around the model by the following method. The flow conditions at the nozzle exit and across the shock wave were computed

from references 5 and 6, respectively. From reference 5 the theoretical rocket performance was computed for several ratios of chamber to exit pressure, the gas composition being assumed to be frozen during the expansion. With each exit condition, the state properties across the normal shock to the model stagnation point were computed from reference 6 by assuming the composition to be in thermochemical equilibrium. The test condition was assumed to be that condition which matched the extrapolated stagnation-point pressure. These results are shown in table VII. The state properties at selected body stations were computed from reference 6 by assuming isentropic flow and by using the measured pressure distribution of figure 7.

With these thermodynamic properties and the transport properties for air (ref. 7), the stagnation-point heating rate was computed by the method of reference 8. For the calculations away from the stagnation point, the flow was considered to be turbulent. The turbulent heating rates were calculated by use of a modified Reynolds analogy and the skin-friction relation of Schultz-Grunow with compressibility effects accounted for by evaluating the flow properties on reference conditions. (See ref. 9.) The calculated heating rates are compared with the measured heating rates in figure 8. The calculated heating rate for the stagnation point does not compare favorably with the extrapolated data. If the accuracy for turbulent heating-rate calculations (ref. 9) is considered, the measured and calculated heating rates for s/r locations greater than 0.7 are in fair agreement.

It should be noted that other investigators (unpublished data) have measured heating rates on similar shaped bodies in the Malta facility which agree with the present experimental data but have computed heating rates which agree with the present computed value of 700 Btu/ft^2-sec (7.95 MW/m^2). Measurements have been made of the noise level of the stream and the results indicate the possibility of the free stream being turbulent. A turbulent free stream can cause a higher stagnation-point heating rate than a laminar free stream. (See ref. 10.)

Prior to the present tests, the stream environment was expected to have a stagnation-point heating rate of 600 to 800 Btu/ft^2-sec (6.8 to 9.1 MW/m^2) and a stagnation pressure of 10 atmospheres. The extrapolated results indicate that the stagnation-point values were 1200 Btu/ft^2-sec (13.60 MW/m^2) for the heating rate and 13 atmospheres for the pressure. Although the actual test environment for the tests of the RAM-CA models was more severe than expected, the flow distribution around the model and the test environment was sufficient to meet the objectives of the test.

ABLATION MODEL RESULTS

There was a burnthrough of the heat shield at the $s/r = 0.8$ location. (See fig. 9.) However, the model was exposed to an extremely severe combustion environment for

23.5 seconds before the burnthrough occurred. As stated in the previous section, the stagnation-point heating rate and pressure were much higher than expected before the test. A comparison between the Malta test environment and the expected flight trajectory for RAM-CA is shown in table VIII. The range of values for K_O, $\dot{m}_O$, and M_O for the test environment is due to uncertainties in the gas reactions with the char layer. For the parameters considered important to char removal $(K_O, \dot{m}_O, M_O, \text{and } p_s)$, the Malta test is seen to be two to three times more severe than the flight environment. It is significant that the ablation model which did not have the final design thicknesses did survive as long as 23.5 seconds as compared with approximately 15 seconds for the time of most severe conditions in flight.

As stated in the Introduction, the primary purpose of the Malta test was to study further some possible problems with the RAM-CA heat shield which could not be completely simulated on small models in the high-enthalpy test facilities at the Langley Research Center. These possible sources of problems are: (1) stagnation-region hole pattern, (2) side-wall hole patterns, (3) Narmco-teflon junction, (4) teflon plugs, three used to cover mechanical connections of the inner shell, (5) mechanical char removal, especially side wall, and (6) overall bonding and assembly. Since the ablation model survived for 23.5 seconds in such a severe environment, this investigation was a good test of these features.

Photographs of the ablation model after testing are shown in figure 9. There was no evidence of problems with any bonding of the heat-shield materials nor with any other heat-shield assembly techniques. Mechanical removal of the Narmco 4028 char occurred in addition to oxidation on the nose of the model back to the hemisphere-cone tangency point. There was no apparent mechanical removal of the char along the side walls. Even though there was mechanical char removal, there was no major damage to the hole pattern at the stagnation region. The side-wall hole patterns were completely unaffected during the test. A rearward-facing step was formed at the Narmco-teflon junction as expected for the test and also expected for the flight. However, there was no evidence of any problem with this formation. Also, there was no problem with the teflon plugs and the behavior of the plugs was the same as that of the teflon in the surrounding areas.

Closeup photographs of the hole patterns after the test are shown in figure 10. As can be seen in the photograph, there was no major problem with the stagnation-hole pattern. Of the 26 holes, only 1 hole in the inner ring and 1 hole in the middle ring showed any enlargement and these two enlargements were not severe. (Also see fig. 11.) This result is very significant since the stagnation area was exposed to a pressure of 13 atmospheres (maximum pressure expected in flight is 11 atmospheres) for 23.5 seconds. As previously stated and as can be seen in the photograph, the side-wall hole patterns were completely unaffected. The front row of the holes ($s/r = 1.30$) was in the region where mechanical char removal occurred.

Photographs of two sectional views of the teflon heat shield are shown in figure 12. In the design of the RAM-CA heat shield, there is a sublayer of teflon in the area aft of the Narmco-teflon junction for added protection because of the formation of a rearward-facing step at the junction caused by the difference of ablation of the two materials. The evidence from this test is that the formation of a rearward-facing step is possible and that the sublayer of teflon is properly located for added protection. The pattern of spots just aft of the Narmco-teflon junction in figure 9 indicates areas where the main layer of teflon was completely ablated and exposed the bond between the main layer and the sublayer. The groove around the teflon heat shield at the midpoint was caused by the stream interference. All the main features of the heat shield to be studied were forward of this location. As previously stated, the stream interference also occurred on the calibration model and was not caused by the step formation.

Sectional views of the Narmco 4028 heat shield are presented in figure 11. As can be seen in the photographs, the most severe mass loss occurred at the location $s/r = 8$. Since this location is a region of high heating and maximum shear, the greater mass loss was expected to occur in this region. A pressure tap ($s/r = 0.78$; $\phi = 180^{o}$) was located in the area where complete burnthrough occurred. However, analysis of the motion-picture film showed that the mechanical char removal was not initiated at the tap location nor propagated around the body from that location. The film data showed the initiation of mechanical char removal to occur simultaneously over the nose region. Although complete burnthrough of the heat shield occurred in the one area, it can be seen that ablation of the heat shield was almost complete at a constant $s/r = 0.8$ around the model. Previous experimental tests at Langley in two materials test facilities have shown Narmco 4028 to have mechanical char removal at pressures greater than 2.5 atmospheres when a significant amount of oxygen is present in the flow stream. Analyses of the Malta model as well as the models tested at Langley have shown that this mechanical removal occurs at the char surface and does not remove the entire char layer at the pyrolysis zone. Therefore, mechanical char removal was expected for the Malta test in the nose region. The thickness of the Narmco 4028 heat shield after the test is given in table II.

As previously mentioned and further illustrated by the photographs of figure 11, there was no apparent mechanical char removal of the Narmco 4028 along the conical side wall. This fact is significant since some previous tests at Malta for the Langley Pacemaker program have shown side-wall spallation for Narmco 4028 and other phenolic-carbon materials. (See ref. 11.) However, a different molding technique and a different fiber orientation are used for the RAM-CA heat shield than for the Pacemaker models. The molding technique for the Narmco 4028 heat shield of the RAM-CA was selected so that the orientation of the fibers would be approximately parallel to the surface around the forward portion of the hemisphere and at an angle of approximately 45^{o} to the surface along the afterbody. However, analysis of the molded heat shield showed the fibers to be

approximately parallel to the surface over the entire body except for two s/r locations along the conical body where the fibers were approximately perpendicular to the surface. The molded billet of the approximate shape was oversized and had to be machined to the required shape and thickness. The Pacemaker models were molded to the required shape and thickness with the fibers parallel to the surface over the entire body. Also, although their shapes are similar, the RAM-CA model is larger than the Pacemaker models. These differences could be the reason for the resistance to side-wall spallation for the RAM-CA model. The experimental ground tests of the small models did not show any side-wall spallation for several types of fiber orientation. Because of the results of the Pacemaker tests at Malta, the possibility of side-wall mechanical char removal in flight was considered to be a major problem area. Therefore, the present test results showing no mechanical side-wall removal were very important.

The results of the thermocouple measurements are given in table IX and are shown in figure 13. None of the thermocouples, except for the stagnation-point thermocouple, indicated any significant temperature rise until the time of the burnthrough. Hence, it could not be determined whether the temperature rises were due to heat soak through the material or from the hot combustion gases which entered the interior of the models. The shape of the temperature-rise curve for the stagnation-point thermocouple (thermocouple 5) is not that normally experienced for an ablator and is not considered to have been the result of heat conduction through the ablative material. A pressure tube was located in the immediate area and would have contained extremely hot gases. It is possible that the thermocouple came in contact with the pressure tube.

The measured surface temperatures of the Narmco 4028 heat shield are shown in figures 14 and 15 for various times and s/r locations. For most of the tests, the surface temperature was approximately 5000° F (3040° K) in the nose region (s/r from 0 to 1.1). For the location of s/r = 0.95 where both the two-color pyrometer and the photographic pyrometer were used, the measured data are in good agreement.

CONCLUDING REMARKS

A full-scale replica of the RAM-CA heat shield was tested at the General Electric Malta test station in order to study some possible problems with the heat-shield design which could not be completely simulated on small models in the materials research test facilities at the Langley Research Center and to serve as a final qualification for the flight heat shield. The possible sources of problems that were studied are the hole patterns at the stagnation region and along the side wall, the junction between the carbon-phenolic material and the teflon, the teflon plugs used to cover mechanical connections, mechanical char removal, and the overall bonding and assembly of the heat-shield structure.

Measurements of the heating rate and pressure distribution were conducted and these measurements along with equilibrium calculation of stream composition provided a definition of the test environment. The test environment was sufficient for an adequate test of the heat-shield features.

There was mechanical char removal in addition to oxidation of the carbon-phenolic material on the hemispherical portion of the model but no apparent mechanical char removal along the conical portion. Of the 26 holes in the hole pattern at the stagnation region, only 2 holes had any enlargement and these enlargements were not severe. The hole patterns along the side wall were completely unaffected. A rearward-facing step was formed at the junction as expected because of differences in ablation of the two materials. However, there was no subsequent problem from the step formation, and the sublayer of teflon was properly located for added protection. The response of the teflon plugs to the test environment was the same as that for the teflon material in the surrounding areas. There was no evidence of problems with any bonding of the heat-shield materials nor of any assembly techniques. The present test results did not show any problems which would disqualify the RAM-CA heat-shield design from flight application.

Langley Research Center,
National Aeronautics and Space Administration,
Langley Station, Hampton, Va., May 15, 1969,
124-08-03-05-23.

REFERENCES

1. Huber, Paul W.; and Sims, Theo E.: The Entry-Communications Problem. Astronaut. Aeron., vol. 2, no. 10, Oct. 1964, pp. 30-40.

2. Sims, Theo E.: Reentry Communications Research at Langley Research Center. IEEE Intern. Conv. Record, vol. 13, pt. 4, 1965, pp. 99-104.

3. Mechtly, E. A.: The International System of Units – Physical Constants and Conversion Factors. NASA SP-7012, 1964.

4. Exton, Reginald J.: Theory and Operation of a Variable Exposure Photographic Pyrometer Over the Temperature Range 1800° to 3600° F (1255° to 2255° K). NASA TN D-2660, 1965.

5. Zeleznik, Frank J.; and Gordon, Sanford: A General IBM 704 or 7090 Computer Program for Computation of Chemical Equilibrium Compositions, Rocket Performance, and Chapman-Jouguet Detonations. NASA TN D-1454, 1962.

6. Zoby, Ernest V.; Kemper, Jane T.; and Jachimowski, Casimir J.: Isentropic Flow Solutions for Reacting Gas Mixtures in Thermochemical Equilibrium. NASA TN D-4114, 1967.

7. Hansen, C. Frederick: Approximations for the Thermodynamic and Transport Properties of High-Temperature Air. NASA TR R-50, 1959. (Supersedes NACA TN 4150.)

8. Cohen, Nathaniel B.: Boundary-Layer Similar Solutions and Correlation Equations for Laminar Heat-Transfer Distribution in Equilibrium Air at Velocities up to 41,100 Feet Per Second. NASA TR R-118, 1961.

9. Zoby, Ernest V.; and Sullivan, Edward M.: Correlation of Free-Flight Turbulent Heat-Transfer Data From Axisymmetric Bodies With Compressible Flat-Plate Relationships. NASA TN D-3802, 1967.

10. Schlichting, Hermann (J. Kestin, trans.): Boundary-Layer Theory. Sixth ed., McGraw-Hill Book Co., 1968.

11. O'Hare, Brian J.: An Analysis of the Spallation of Carbon Phenolic Ablators. M.S. Thesis, Virginia Polytech. Inst., June 1967.

TABLE I.- ABLATION-MODEL COORDINATE SYSTEM AND LOCATION OF ESSENTIAL FEATURES

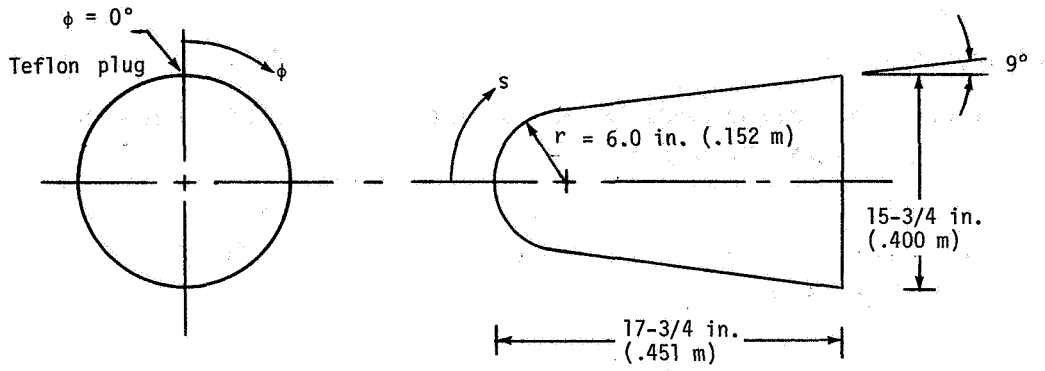

Feature	Essential features	
	s/r location	Element, ϕ, deg
Stagnation-hole pattern	0	0
Side-wall hole pattern (2 sets)	1.30 to 1.78	90, 270
Teflon plugs (3)	2.20	0, 120, 240
Narmco-teflon junction	2.12	----------

Pressure sensors located at $\phi = 180^{o}$ and s/r of –
0.05
.52
.78
1.05
1.41
2.01

Thermocouple	Location of thermocouples	
	ϕ, deg	s/r
1	45	1.88
2	45	1.41
3	45	.78
4	45	.39
5	0	0
6	225	.39
7	225	.78
8	225	1.41
9	225	1.88
10	315	1.88
11	315	1.41
12	315	.78
13	315	.39

Thermocouple	Location of thermocouples	
	ϕ, deg	s/r
14	135	0.39
15	135	.78
16	135	1.41
17	135	1.88
18	135	2.26
19	135	2.44
20	225	2.26
21	225	2.44
22	315	2.26
23	315	2.44
24	45	2.26
25	45	2.44

TABLE II.- THICKNESS OF NARMCO 4028 BEFORE AND AFTER TEST

Condition	Thickness at s/r of –											
	0	0.17	0.35	0.52	0.70	0.79	0.87	1.05	1.22	1.41	1.76	2.11
Virgin material before test, in. (cm)	0.91 (2.31)	0.90 (2.29)	0.89 (2.26)	0.85 (2.16)	0.82 (2.08)	0.80 (2.03)	0.78 (1.98)	0.73 (1.85)	0.66 (1.68)	0.58 (1.47)	0.54 (1.37)	0.49 (1.24)
$\phi = 75^{o}$:												
Virgin material after test, in. (cm)	0.32 (0.81)	0.26 (0.66)	0.15 (0.38)	0.09 (0.23)	0	0	0.01 (0.03)	0.18 (0.46)	0.33 (0.84)	0.36 (0.91)	0.26 (0.66)	0.19 (0.48)
Char layer thickness, in. (cm)	0.10 (0.25)	0.14 (0.35)	0.17 (0.43)	0	0	0	0.04 (0.10)	0.06 (0.15)	0.11 (0.28)	0.18 (0.46)	0.20 (0.51)	0.27 (0.68)
$\phi = 165^{o}$:												
Virgin material after test, in. (cm)	0.32 (0.81)	0.21 (0.53)	0.04 (0.10)	0	0	0	0	0.23 (0.58)	0.36 (0.91)	0.34 (0.86)	0.25 (0.64)	0.24 (0.61)
Char layer thickness, in. (cm)	0.10 (0.25)	0.11 (0.28)	0.04 (0.10)	0	0	0	0	0.06 (0.15)	0.14 (0.36)	0.20 (0.51)	0.23 (0.58)	0.24 (0.61)
$\phi = 255^{o}$:												
Virgin material after test, in. (cm)	0.32 (0.81)	0.20 (0.51)	0.09 (0.23)	0	0	0	0.02 (0.05)	0.17 (0.43)	0.35 (0.89)	0.37 (0.94)	0.15 (0.38)	0.20 (0.51)
Char layer thickness, in. (cm)	0.10 (0.25)	0.06 (0.15)	0	0	0	0	0	0.03 (0.08)	0.11 (0.28)	0.19 (0.48)	0.30 (0.76)	0.26 (0.66)
$\phi = 345^{o}$:												
Virgin material after test, in. (cm)	0.32 (0.81)	0.17 (0.43)	0.10 (0.25)	0.06 (0.15)	0.02 (0.05)	0.01 (0.03)	0.04 (0.10)	0.15 (0.38)	0.32 (0.81)	0.35 (0.89)	0.30 (0.76)	0.20 (0.51)
Char layer thickness, in. (cm)	0.10 (0.25)	0.07 (0.18)	0.05 (0.13)	0.04 (0.10)	0.04 (0.10)	0.05 (0.13)	0.02 (0.05)	0.06 (0.15)	0.06 (0.15)	0.18 (0.46)	0.18 (0.46)	0.22 (0.56)

TABLE III.- LOCATIONS OF HEATING-RATE AND PRESSURE SENSORS ON CALIBRATION MODEL

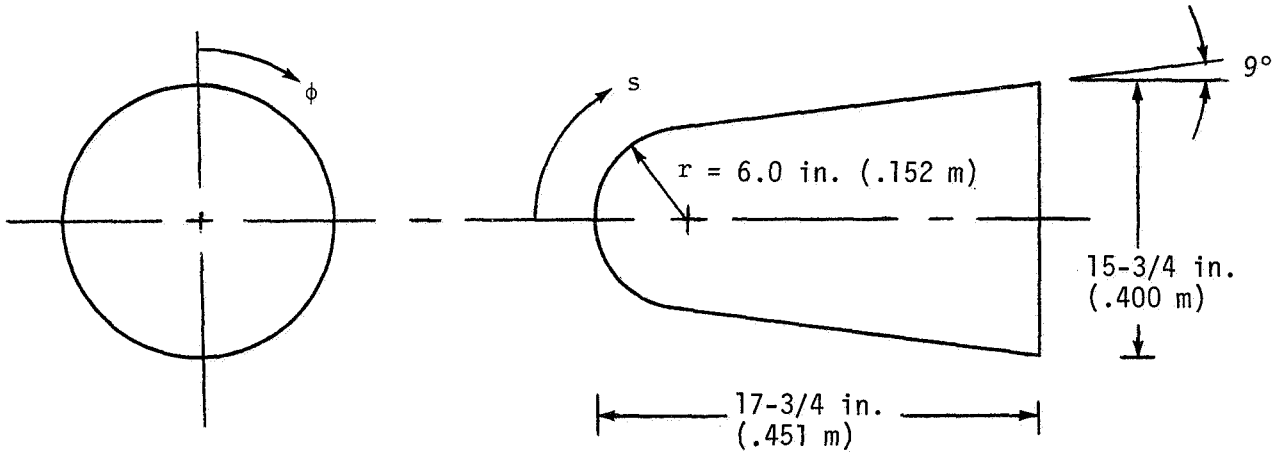

Heating-rate sensors

s/r at –	
$\phi = 0^{o}$	$\phi = 180^{o}$
0	0.78
.39	1.22
.78	
1.10	
1.41	
2.01	

Pressure sensors

s/r at $\phi = 90^{o}$
0.17
.52
.78
1.05
1.22
1.41
2.01

TABLE IV.- ROCKET ENGINE FIRING DATA

[Malta test facility no. 4; oxidizer, liquid oxygen; fuel, ethyl alcohol]

Calibration model; test run 297M4; test date, August 17, 1966:		
Chamber pressure, psia (atm)	582	(39.6)
Oxidizer-to-fuel weight ratio	1.9871	
Oxidizer flow rate, lbm/sec (kg/sec)	73.4	(33.3)
Fuel flow rate, lbm/sec (kg/sec)	36.9	(16.8)
Oxidizer specific gravity	1.1438	
Fuel specific gravity	0.8166	
Oxidizer inlet temperature, ^{o}F (^{o}K)	-292.5	(93.1)
Fuel inlet temperature, ^{o}F (^{o}K)	65.4	(291.9)
Ablation test model; test run 298M4; test date, August 19, 1966:		
Chamber pressure, psia (atm)	571	(38.9)
Oxidizer-to-fuel weight ratio	2.001	
Oxidizer flow rate, lbm/sec (kg/sec)	73.5	(33.4)
Fuel flow rate, lbm/sec (kg/sec)	36.7	(16.7)
Oxidizer specific gravity	1.1439	
Fuel specific gravity	0.8153	
Oxidizer inlet temperature, ^{o}F (^{o}K)	-292.5	(93.1)
Fuel inlet temperature, ^{o}F (^{o}K)	68.1	(293.4)

TABLE V.- RESULTS OF MEASURED PRESSURE DISTRIBUTION

s/r location	Pressure, atm for –	
	Calibration model	Ablation model
0.05	----	12.23
.17	12.31	----
.52	7.83	8.51
.78	5.51	5.37
1.05	2.86	2.31
1.22	1.50	----
1.41	.82	.95
2.01	.88	.67

TABLE VI.- RESULTS OF MEASURED HEATING-RATE DISTRIBUTION

s/r location	Heating rate,
	Btu/ft^2-sec $\left(MW/m^2\right)$
$\phi = 0^o$	
0	No data
.39	1125 (12.78)
.78	1105 (12.53)
1.10	674 (7.65)
1.41	247 (2.80)
2.01	382 (4.34)
$\phi = 180^o$	
0.78	953 (10.80)
1.22	380 (4.31)

TABLE VII.- CALCULATED FLOW CONDITIONS

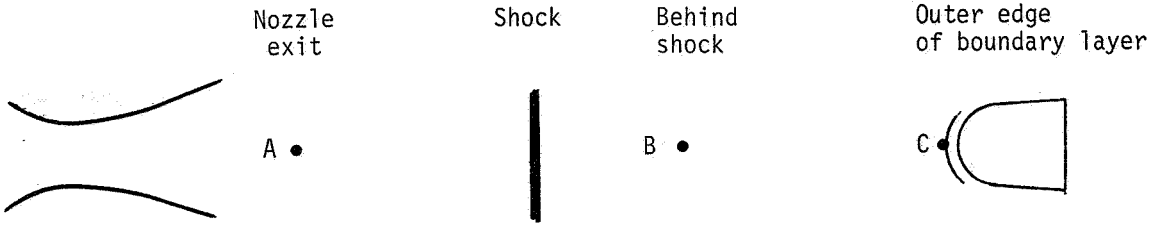

Point A		Point B		Point C	
V_1 = 7830 ft/sec (2386 m/s) T_1 = 3550° R (1970° K) p_1 = 1.5 atm		V_2 = 1618 ft/sec (493 m/s) T_2 = 5500° R (3060° K) p_2 = 11.7 atm		T_T = 5550° R (3080° K) p_s = 13.0 atm	
Gas	Mole fraction	Gas	Mole fraction	Gas	Mole fraction
H_2O	0.446	H_2O	0.323	H_2O	0.319
CO_2	.196	CO_2	.236	CO_2	.233
CO	.129	CO	.079	CO	.080
O_2	.082	O_2	.126	O_2	.128
OH	.077	OH	.043	OH	.044
H_2	.037	H_2	.154	H_2	.156
O	.017	O	.015	O	.015
H	.014	H	.023	H	.024

TABLE VIII.- STAGNATION-POINT COMPARISON BETWEEN MALTA TEST ENVIRONMENT AND NOMINAL RAM-CA FLIGHT ENVIRONMENT

Condition	Flight		Malta; t = 23.5 seconds
	Maximum	Average	
Composition	Air	Air	Combustion products
$\dot{q}_s$, Btu/ft^2-sec (MW/m^2)	1800 (20.4)	570 (6.5)	1200 (13.6)
Q_s, Btu/ft^2 (MJ/m^2)	28 500 (324)	----------	27 600 (314)
p_s, atm	11	2.7	13
K_O	0.23	----------	0.4 to 0.6
$\dot{m}_O$, lbm/ft^2-sec (kg/m^2-s)	0.056 (0.274)	0.020 (0.098)	0.13 to 0.21 (0.64 to 1.03)
M_O, lbm/ft^2 (kg/m^2)	1.02 (4.99)	----------	3.0 to 4.9 (14.7 to 24.0)

TABLE IX.- RESULTS OF THERMOCOUPLES ON ABLATION MODEL

End of exposure to rocket exhaust was 23.5 seconds.
Thermocouples 17, 21, and 23 did not deflect during the test.
Thermocouples 18, 19, 22, 24, and 25 had sensitive calibration and deflected off the oscillograph record at approximately 23.55 seconds. The thermocouples returned at 28.5 seconds with a smooth trace.
Thermocouples 5, 7, and 20 deflected off scale and returned between 24 and 29 seconds.

Time, sec	Temperature, °F (°K) for thermocouples –															
	1	2	3	4	6	8	9	10	11	12	13	14	15	16
0	71 (295)	71 (295)	71 (295)	71 (295)	71 (295)	71 (295)	71 (295)	71 (295)	71 (295)	71 (295)	71 (295)	71 (295)	71 (295)	69 (294)
2.5	71 (295)	71 (295)	71 (295)	71 (295)	71 (295)	71 (295)	71 (295)	71 (295)	71 (295)	71 (295)	71 (295)	71 (295)	71 (295)	69 (294)
5.5	71 (295)	71 (295)	71 (295)	71 (295)	71 (295)	71 (295)	71 (295)	71 (295)	71 (295)	71 (295)	71 (295)	71 (295)	71 (295)	69 (294)
8.5	71 (295)	71 (295)	71 (295)	71 (295)	72 (296)	71 (295)	71 (295)	71 (295)	71 (295)	71 (295)	71 (295)	71 (295)	71 (295)	69 (294)
11.5	71 (295)	71 (295)	71 (295)	71 (295)	74 (297)	71 (295)	71 (295)	71 (295)	71 (295)	71 (295)	71 (295)	72 (296)	71 (295)	69 (294)
14.5	71 (295)	71 (295)	72 (296)	71 (295)	75 (297)	71 (295)	71 (295)	72 (296)	71 (295)	73 (296)	72 (296)	74 (297)	71 (295)	70 (294)
18.5	72 (296)	71 (295)	73 (296)	71 (295)	78 (299)	71 (295)	73 (296)	75 (297)	72 (296)	71 (295)	71 (295)	74 (297)	71 (295)	70 (294)
21.5	75 (297)	72 (296)	73 (296)	71 (295)	81 (301)	72 (296)	78 (299)	79 (299)	72 (296)	74 (297)	72 (296)	75 (297)	73 (296)	70 (294)
22.5	75 (297)	72 (296)	81 (301)	74 (297)	82 (301)	72 (296)	79 (299)	81 (301)	72 (296)	80 (300)	74 (297)	76 (298)	74 (297)	71 (295)
23.5	99 (311)	83 (302)	109 (316)	75 (297)	82 (301)	80 (300)	91 (306)	103 (313)	79 (299)	101 (312)	67 (293)	76 (298)	77 (298)	70 (294)
23.6	105 (314)	92 (307)	122 (323)	75 (297)	83 (302)	81 (301)	96 (309)	108 (316)	81 (301)	104 (313)	78 (299)	78 (299)	78 (299)	72 (296)
24.5	144 (336)	160 (344)	139 (333)	162 (346)	90 (306)	113 (318)	101 (312)	158 (343)	126 (326)	159 (344)	92 (307)	79 (299)	114 (319)	74 (297)
25.9	152 (340)	331 (439)	267 (404)	105 (314)	99 (311)	129 (327)	138 (322)	175 (353)	137 (332)	199 (366)	121 (323)	81 (301)	162 (346)	75 (297)
28.5	158 (343)	265 (403)	287 (415)	142 (334)	101 (312)	136 (331)	149 (338)	186 (359)	143 (335)	260 (400)	151 (339)	84 (302)	217 (376)	76 (298)
33.5	166 (348)	200 (367)	277 (409)	172 (351)	107 (315)	139 (333)	166 (348)	197 (365)	144 (336)	315 (431)	171 (351)	83 (302)	239 (388)	78 (299)
38.5	179 (355)	165 (347)	269 (405)	181 (356)	118 (321)	145 (336)	189 (361)	218 (377)	146 (337)	325 (436)	181 (356)	85 (303)	241 (389)	79 (299)
43.5	196 (364)	160 (344)	263 (402)	184 (358)	156 (342)	150 (339)	213 (374)	236 (387)	149 (338)	318 (432)	184 (358)	83 (302)	267 (404)	75 (297)
48.5	216 (376)	167 (348)	260 (400)	186 (359)	164 (347)	157 (343)	238 (388)	257 (398)	156 (342)	310 (428)	186 (359)	83 (302)	260 (400)	75 (297)
53.5	231 (384)	176 (353)	257 (398)	187 (359)	170 (350)	166 (348)	259 (399)	274 (408)	163 (346)	305 (425)	188 (360)	84 (302)	269 (405)	74 (297)
58.5	252 (396)	187 (359)	254 (397)	188 (360)	178 (354)	176 (353)	282 (412)	293 (418)	173 (352)	297 (421)	189 (361)	83 (302)	240 (389)	75 (297)
63.5	272 (407)	200 (367)	251 (395)	188 (360)	187 (359)	187 (359)	303 (424)	311 (428)	183 (357)	292 (418)	190 (361)	83 (302)	279 (411)	75 (297)
68.5	290 (417)	213 (374)	249 (394)	189 (361)	193 (363)	200 (367)	322 (434)	327 (437)	195 (364)	285 (414)	190 (361)	83 (302)	259 (399)	77 (298)
73.5	305 (425)	225 (381)	246 (392)	188 (360)	198 (366)	212 (373)	339 (444)	346 (448)	206 (370)	280 (411)	191 (362)	83 (302)	269 (405)	77 (298)
78.5	320 (433)	241 (389)	244 (391)	188 (360)	206 (370)	223 (379)	353 (452)	354 (452)	217 (376)	273 (407)	190 (361)	83 (302)	230 (383)	75 (297)
88.5	346 (448)	261 (401)	240 (389)	189 (361)	245 (392)	247 (393)	377 (465)	375 (464)	237 (387)	263 (402)	189 (361)	83 (302)	248 (393)	75 (297)
98.5	365 (458)	283 (413)	231 (384)	189 (361)	245 (392)	269 (405)	393 (474)	389 (472)	264 (402)	247 (393)	195 (364)	77 (298)	292 (418)	77 (298)
108.5	379 (466)	296 (420)	231 (384)	190 (361)	246 (392)	288 (416)	404 (480)	398 (477)	276 (409)	243 (391)	189 (361)	81 (301)	302 (423)	78 (299)

TABLE IX.- RESULTS OF THERMOCOUPLES ON ABLATION MODEL – Concluded

Time, sec	Temperature, °F (°K) for thermocouple –									
	18		19		22		24		25	
0	71	(295)	77	(298)	71	(295)	71	(295)	71	(295)
2.5	71	(295)	77	(298)	71	(295)	71	(295)	71	(295)
5.5	71	(295)	77	(298)	72	(296)	71	(295)	71	(295)
8.5	73	(296)	79	(299)	75	(297)	74	(297)	74	(297)
11.5	74	(297)	82	(301)	76	(298)	75	(297)	77	(298)
14.5	76	(298)	84	(302)	78	(299)	76	(298)	81	(301)
18.5	80	(300)	88	(304)	85	(303)	81	(301)	86	(303)
21.5	82	(301)	91	(306)	90	(306)	85	(303)	89	(305)
22.5	84	(302)	93	(307)	92	(307)	180	(356)	91	(306)
23.0	86	(303)	104	(313)	119	(322)	110	(317)	105	(314)
23.4	132	(329)	141	(334)	167	(348)	165	(347)	138	(332)
23.5	161	(345)	172	(351)	187	(359)	180	(356)	154	(341)
23.55	270	(406)	249	(394)	231	(384)	212	(373)	205	(369)
28.5	904	(758)	984	(802)	852	(729)	880	(744)	850	(728)
33.5	615	(597)	646	(614)	548	(560)	581	(578)	553	(563)
38.5	448	(504)	456	(509)	395	(475)	421	(489)	412	(484)
43.5	380	(467)	383	(468)	331	(439)	405	(481)	347	(448)
48.5	344	(447)	347	(448)	296	(420)	294	(419)	311	(428)
53.5	319	(433)	321	(434)	276	(409)	294	(419)	387	(415)
58.5	298	(421)	301	(423)	262	(401)	279	(411)	271	(406)
63.5	280	(411)	275	(408)	250	(394)	266	(403)	259	(399)
68.5	265	(403)	272	(407)	240	(389)	256	(398)	249	(394)
73.5	246	(392)	279	(411)	234	(386)	246	(392)	239	(388)
78.5	237	(387)	248	(393)	230	(383)	240	(389)	232	(384)
88.5	223	(379)	295	(419)	222	(379)	232	(384)	223	(379)
98.5	214	(374)	281	(412)	214	(374)	223	(379)	213	(374)
100.5	214	(374)	279	(411)	208	(371)	219	(377)	206	(370)

Time, sec	Temperature, °F (°K) for thermocouple –					
	5		7		20	
0	68	(293)	67	(293)	65	(292)
.5	68	(293)	67	(293)	65	(292)
2.5	112	(318)	67	(293)	65	(292)
4.5	143	(335)	67	(293)	65	(292)
6.5	165	(347)	67	(293)	67	(293)
8.5	184	(358)	67	(293)	68	(293)
10.5	199	(366)	67	(293)	69	(294)
12.5	213	(374)	67	(293)	72	(296)
14.5	225	(381)	67	(293)	73	(296)
16.5	237	(387)	67	(293)	74	(297)
18.5	248	(393)	68	(293)	75	(297)
20.5	258	(399)	69	(294)	77	(298)
21.5	267	(404)	72	(296)	78	(299)
22.5	278	(410)	86	(303)	79	(299)
23.5	291	(417)	275	(408)	86	(303)
24.5	Off scale		1062	(846)	1083	(857)
29.5	299	(422)	822	(712)	904	(758)
33.5	267	(404)	757	(676)	673	(629)
38.5	241	(389)	695	(642)	496	(531)
43.5	221	(378)	647	(615)	403	(479)
48.5	212	(373)	660	(622)	338	(443)
53.5	208	(371)	574	(574)	294	(419)
58.5	204	(369)	543	(557)	262	(401)
63.5	203	(368)	520	(544)	240	(389)
68.5	204	(369)	497	(532)	222	(379)
73.5	205	(369)	474	(519)		
78.5	209	(372)				

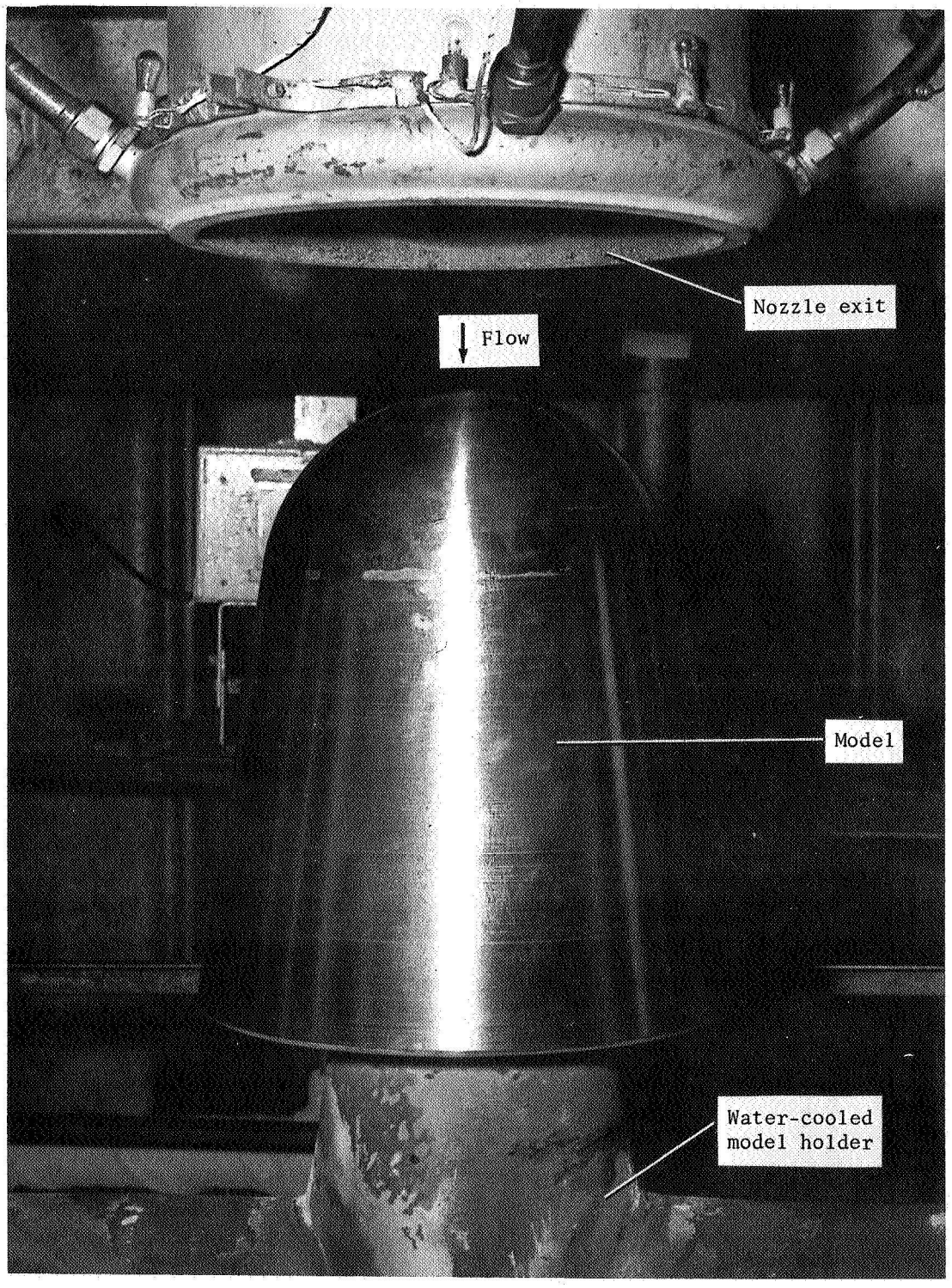

Figure 1.- Photograph of the nozzle's exit and a model in position for a test. L-69-1385

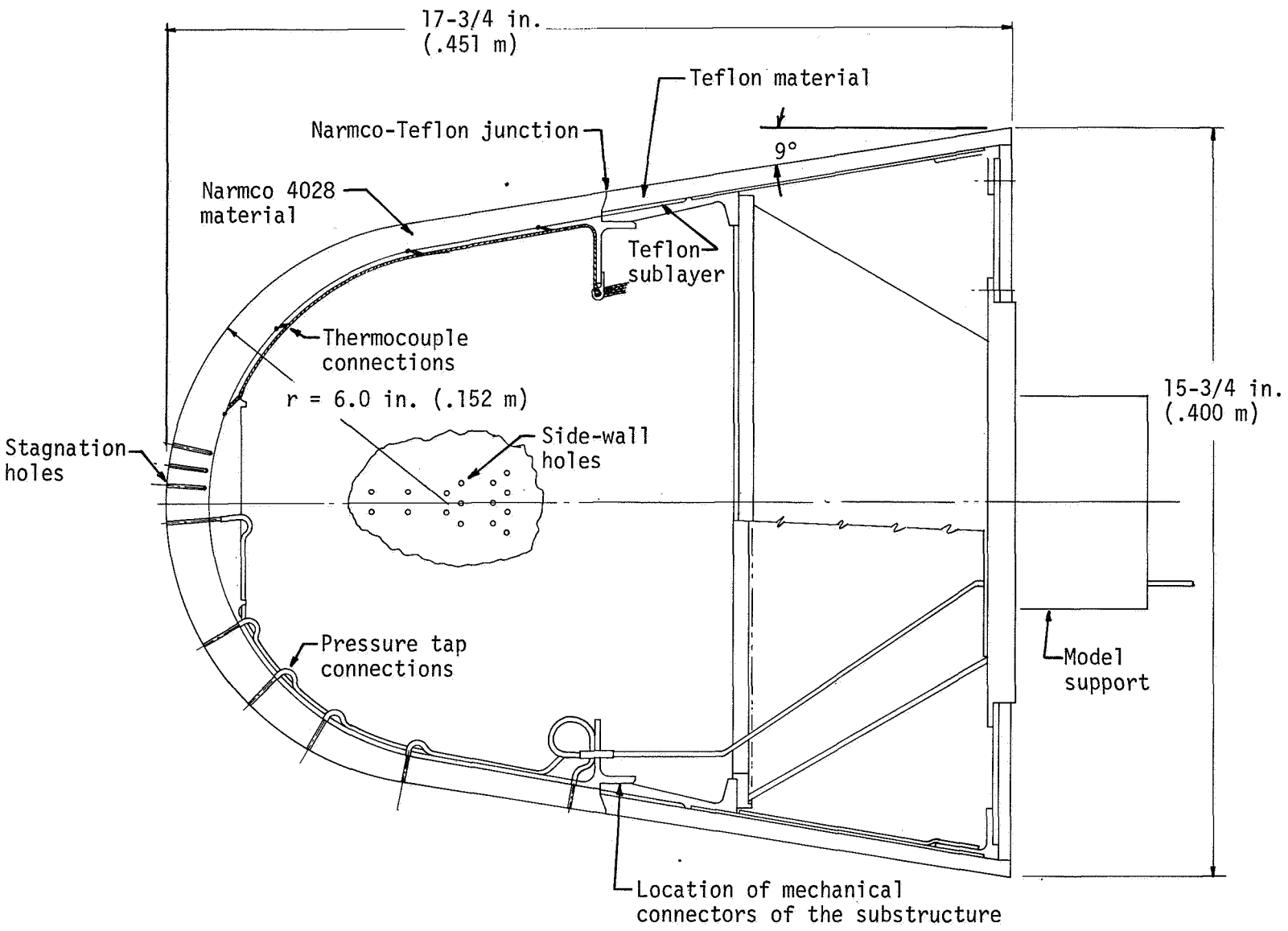

Figure 2.- Drawing of ablation model.

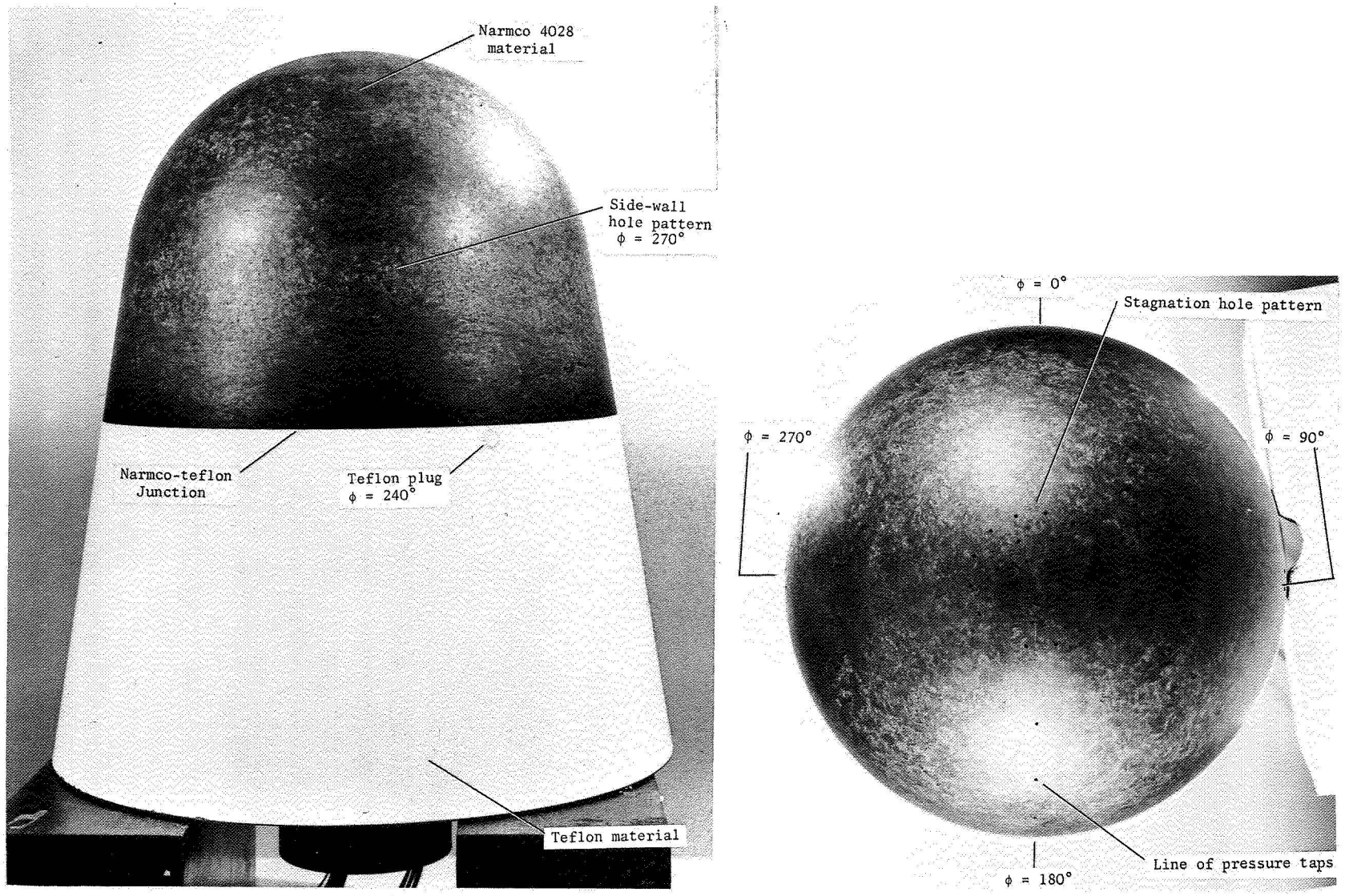

(a) Side view.

(b) Top view.

Figure 3.- Photographs of the ablation model before test.

L-69-1386

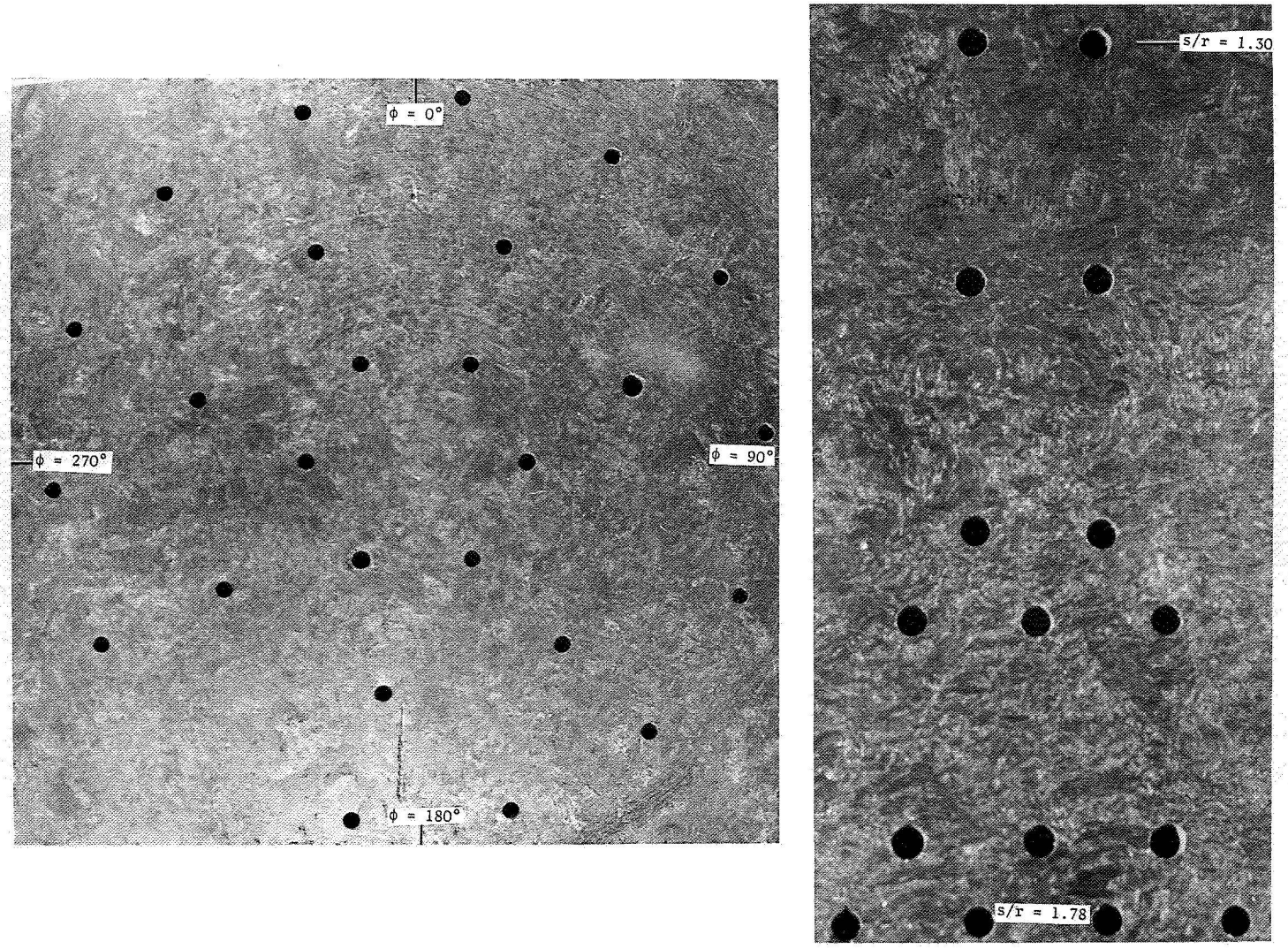

(a) Stagnation hole pattern.

(b) Side-wall hole pattern.

Figure 4.- Closeup photographs of hole patterns before test. L-69-1387

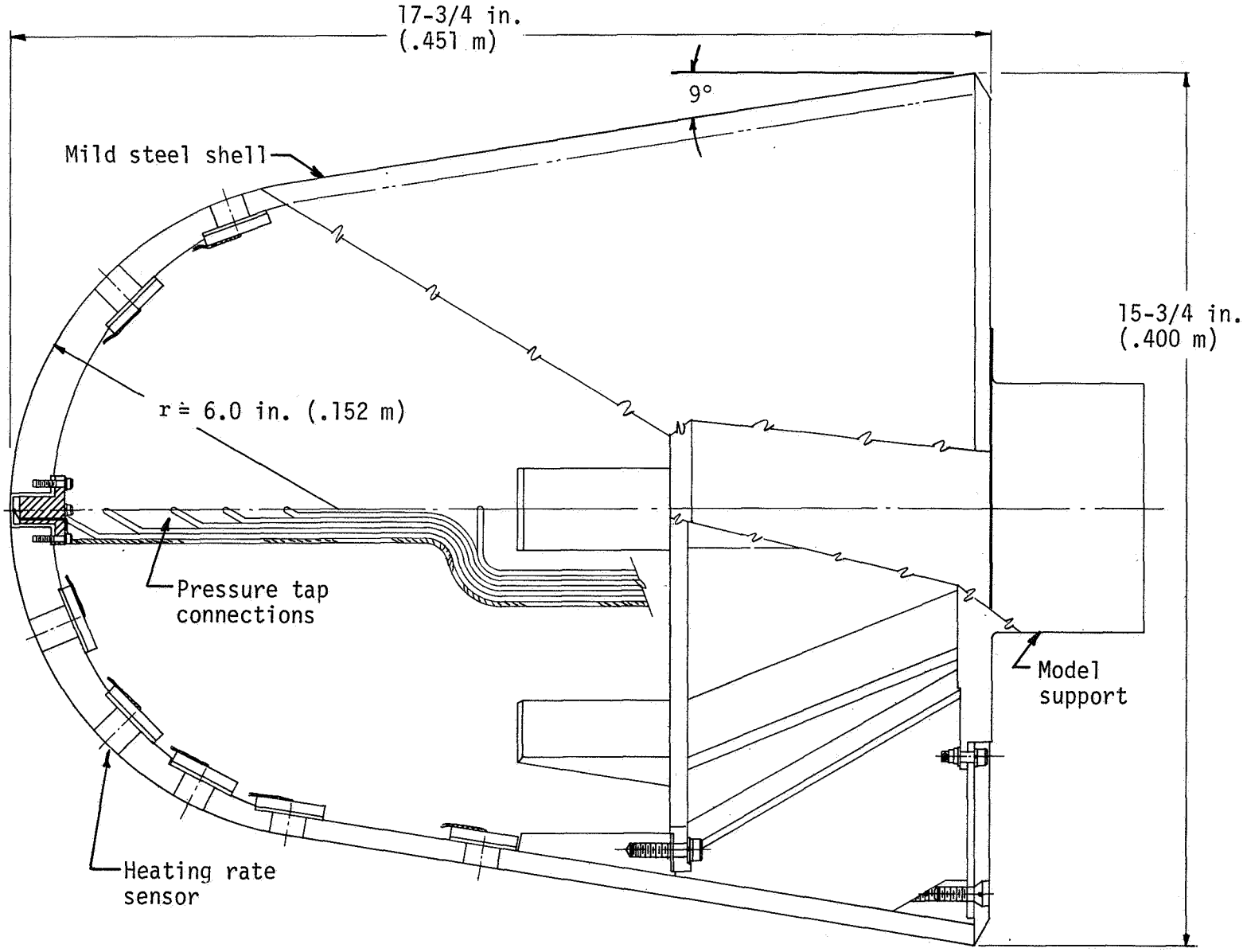

Figure 5.- Drawing of calibration model.

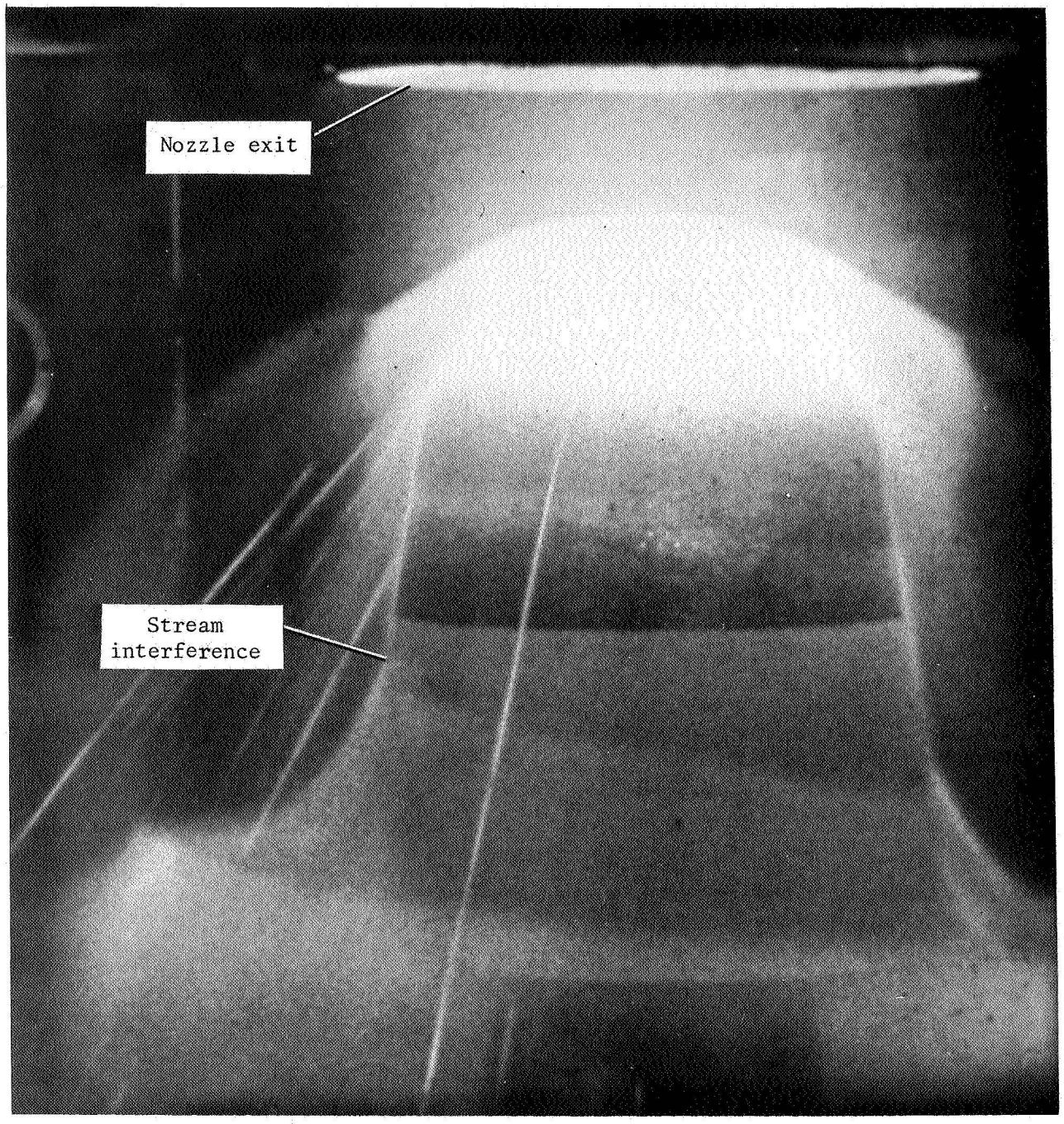

Figure 6.- Photograph showing stream interference on ablation model. L-69-1388

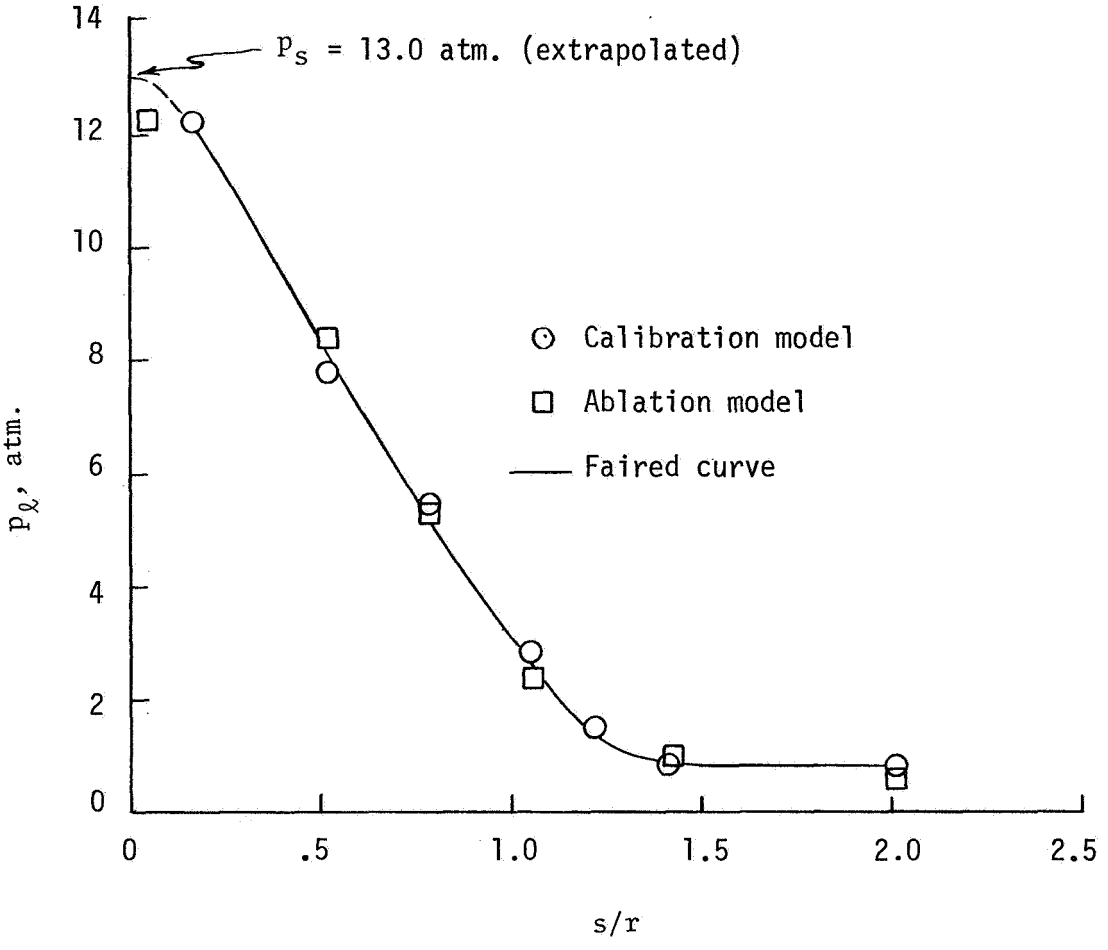

Figure 7.- Results of measured pressure distribution.

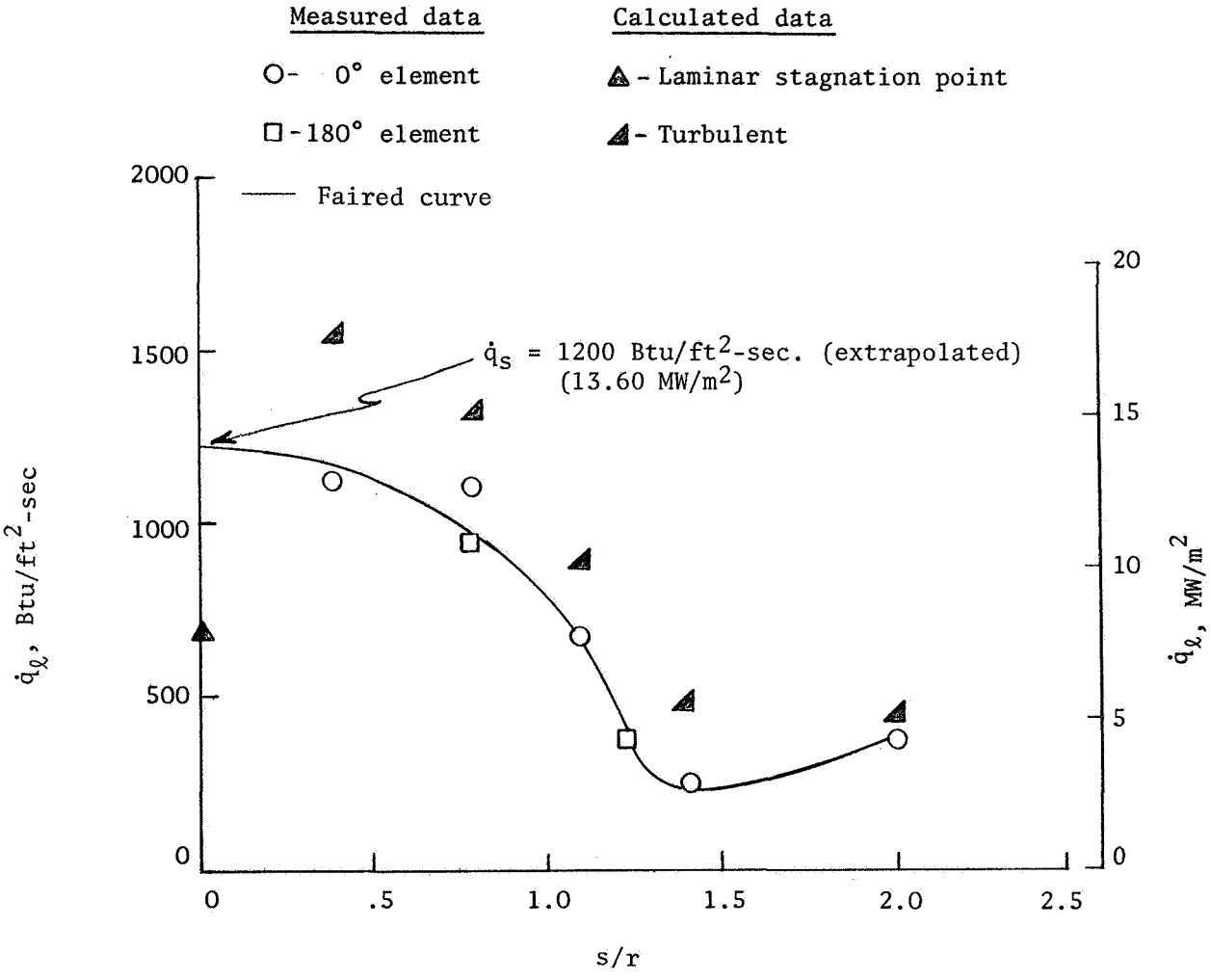

Figure 8.- Results of the measured and calculated heating-rate distribution.

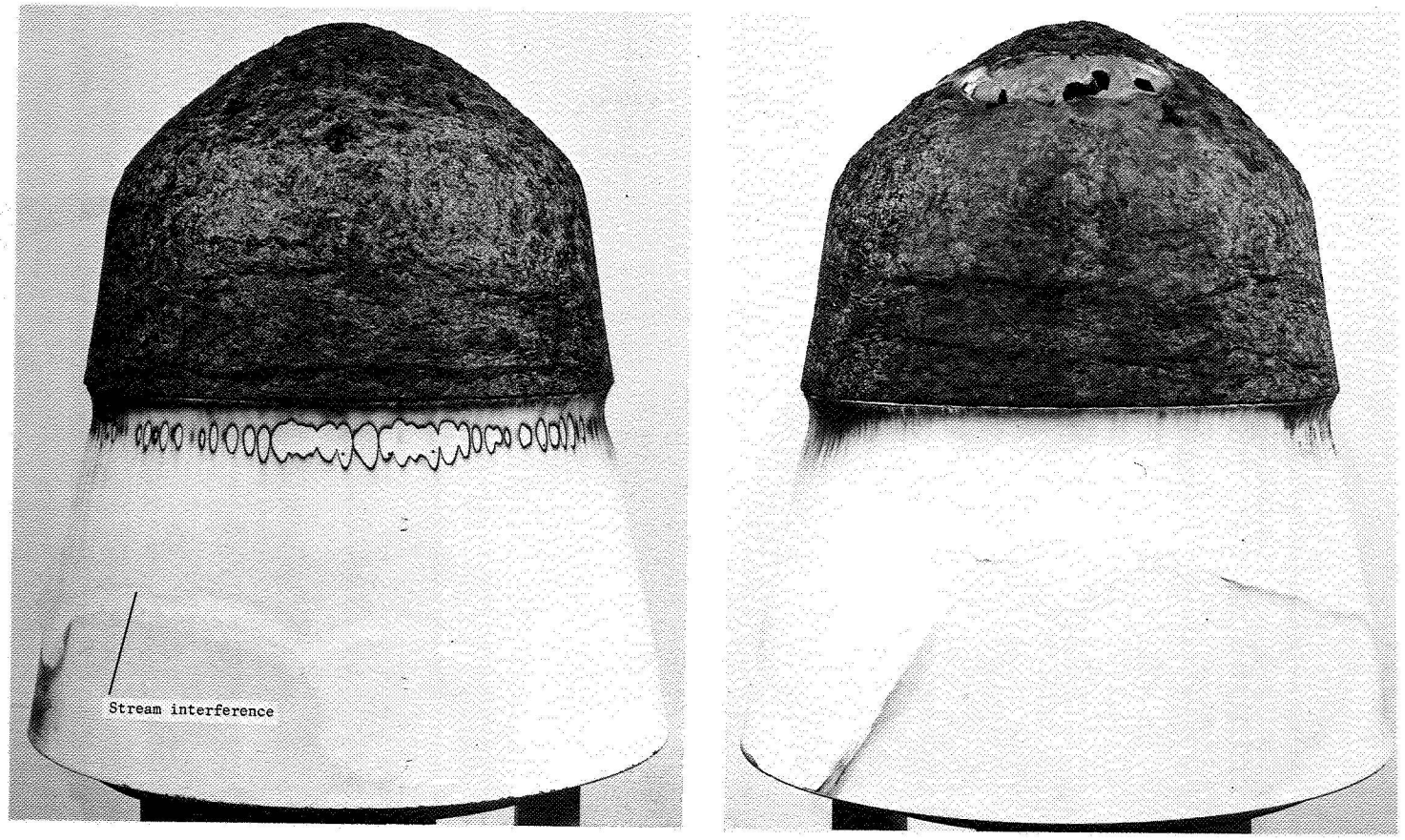

(a) Side view at element $\phi = 0^{0}$.

(b) Side view at element $\phi = 180^{0}$.

Figure 9.- Photographs of ablation model after test. L-69-1389

(c) Side view at element $\Phi = 270^{0}$.

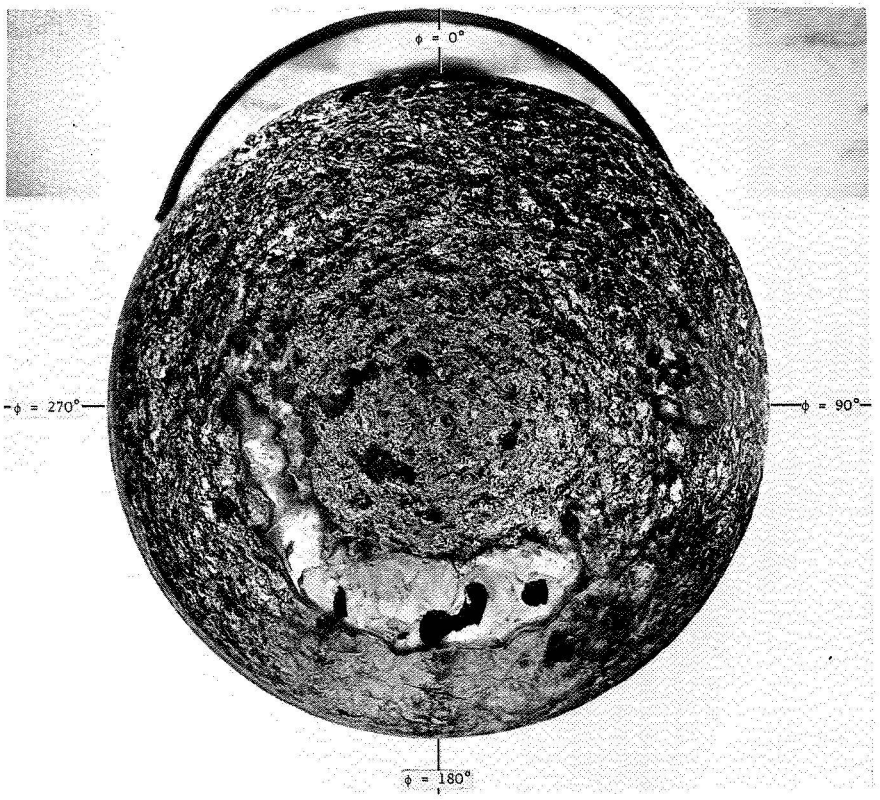

(d) Top view.

Figure 9.- Concluded.

L-69-1390

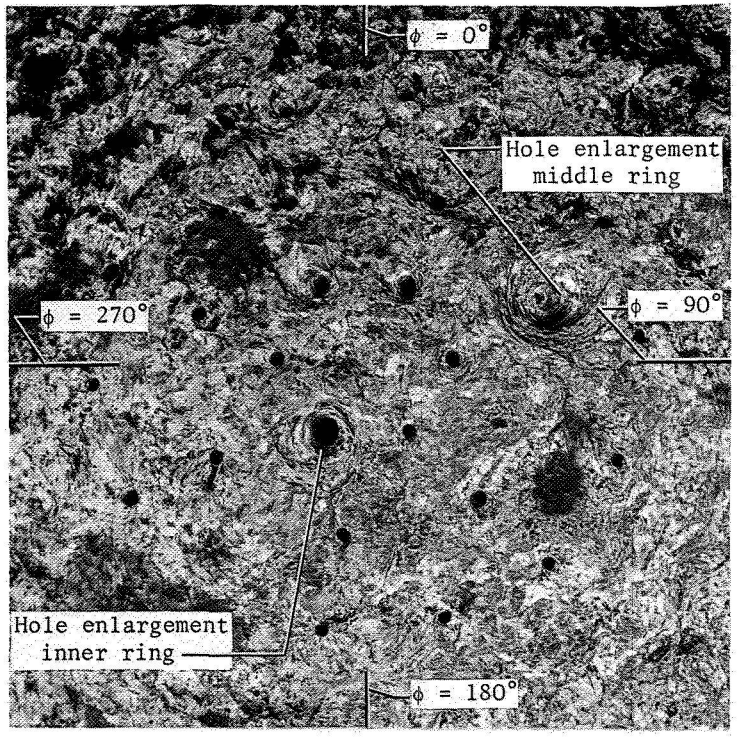

(a) Stagnation hole pattern.

(b) Side-wall hole pattern at element $\Phi = 90^0$.

Figure 10.- Closeup photographs of hole patterns after test.

L-69-1391

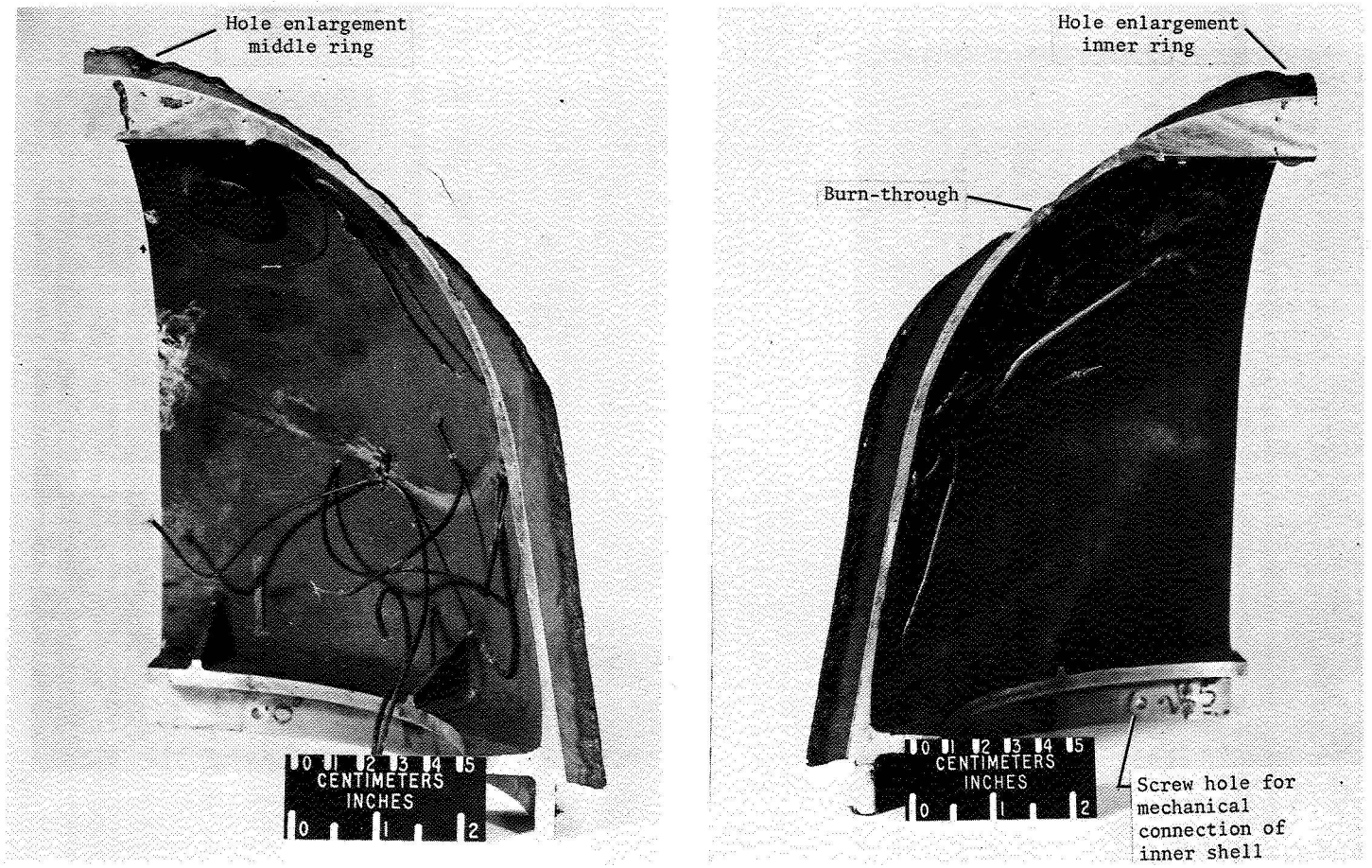

(a) Element $\Phi = 75^{0}$.

(b) Element $\Phi = 165^{0}$.

Figure 11.- Sectional views of Narmco 4028 heat shield after test.

L-69-1392

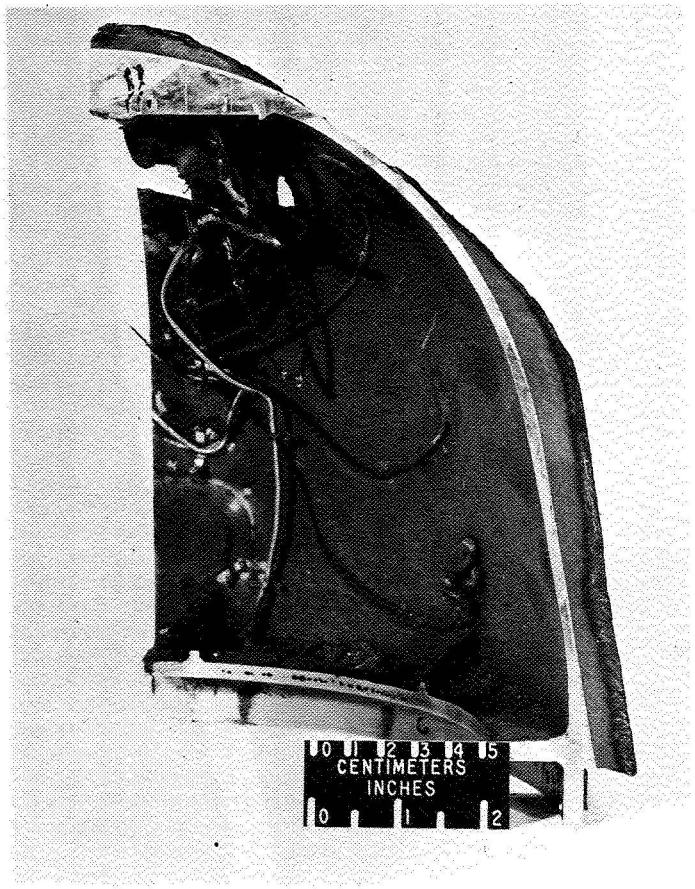

(c) Element $\phi = 255^{o}$.

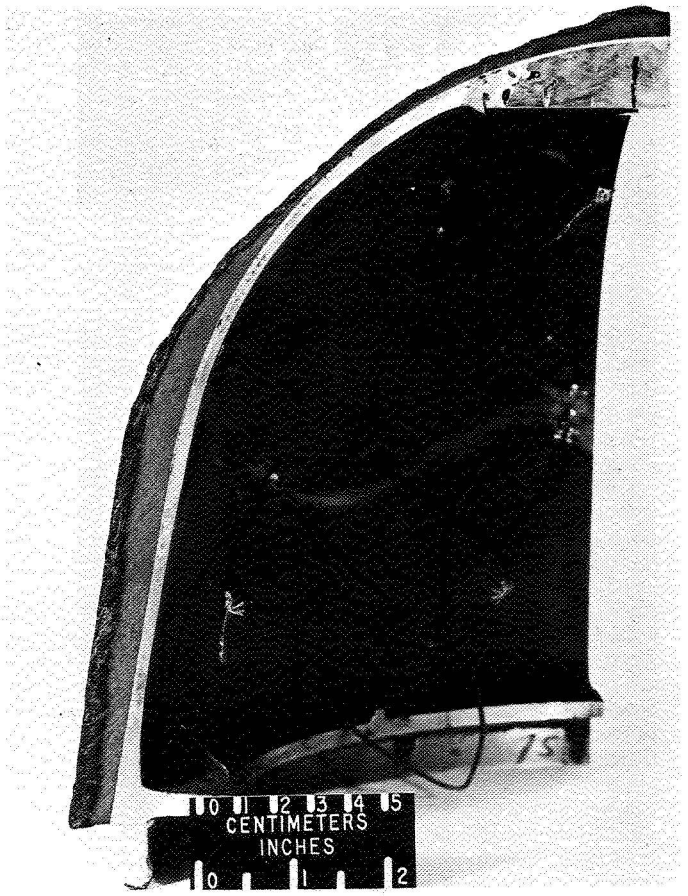

(d) Element $\phi = 345^{o}$.

Figure 11.- Concluded.

L-69-1393

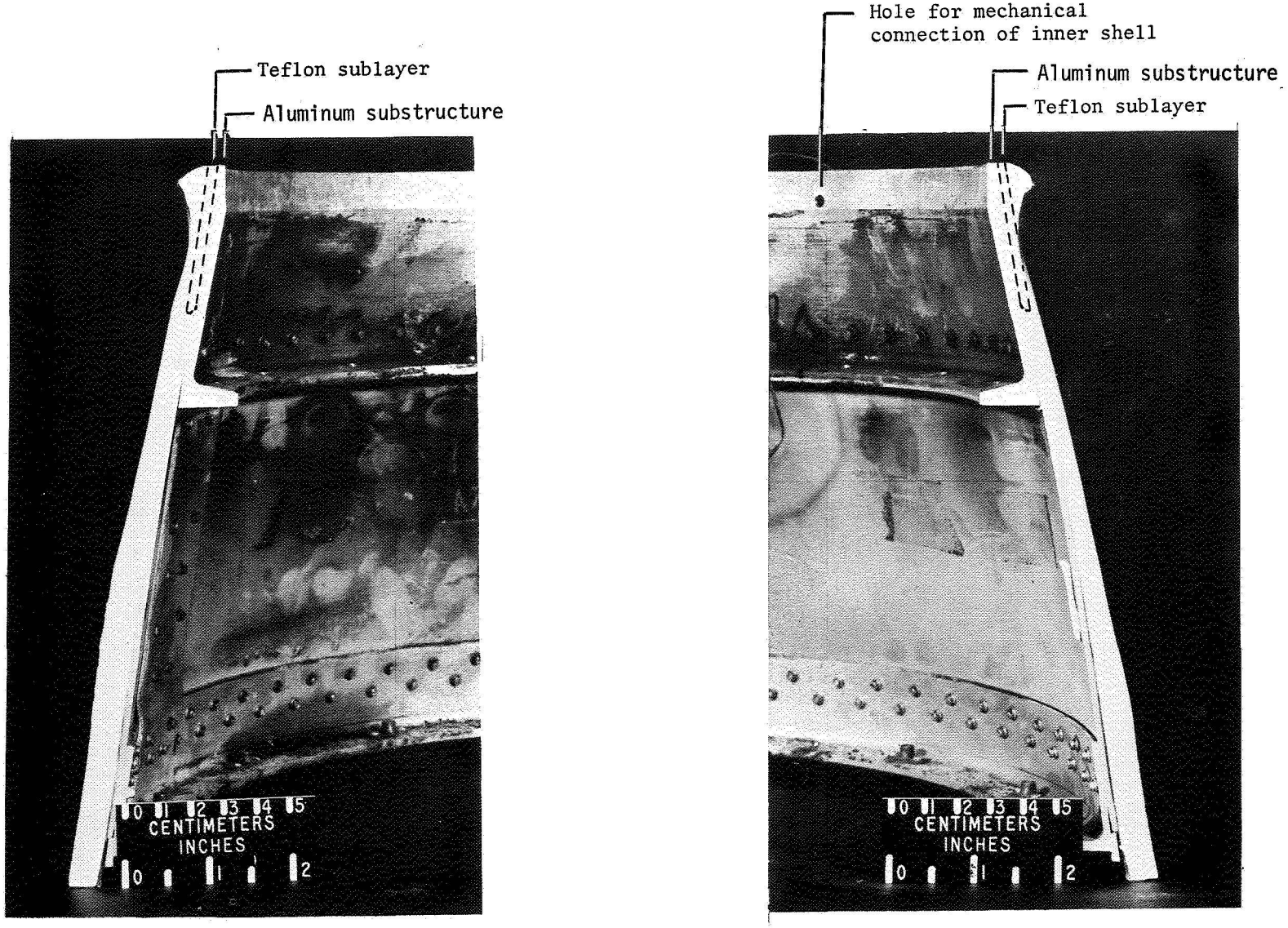

(a) Element $\Phi = 110^{0}$.

(b) Element $\Phi = 290^{0}$.

Figure 12.- Sectional views of teflon heat shield after test.

L-69-1394

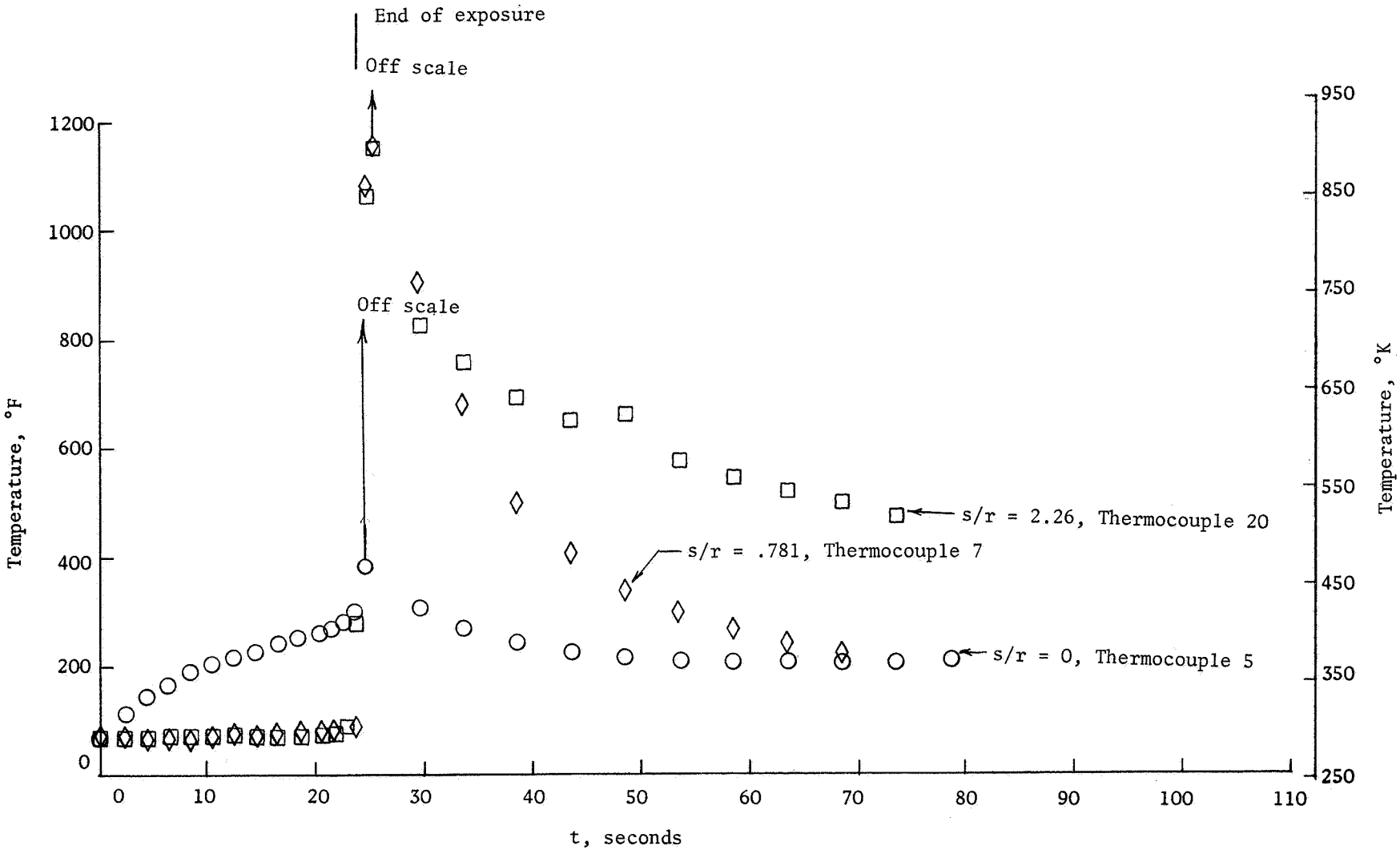

(a) Element $\Phi = 225^0$.

Figure 13.- Results from thermocouples on ablation model.

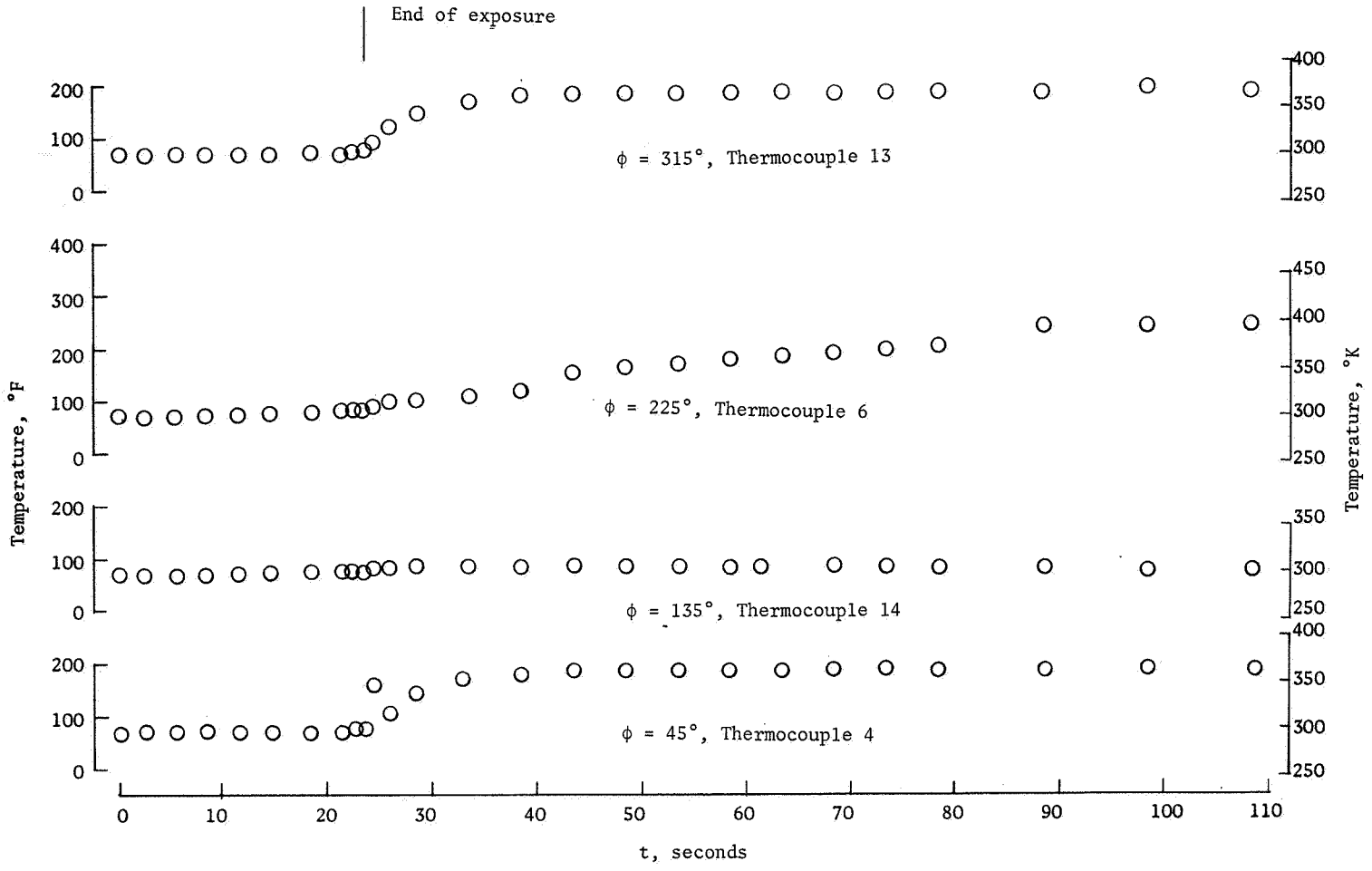

(b) Location s/r = 0.39.

Figure 13.- Continued.

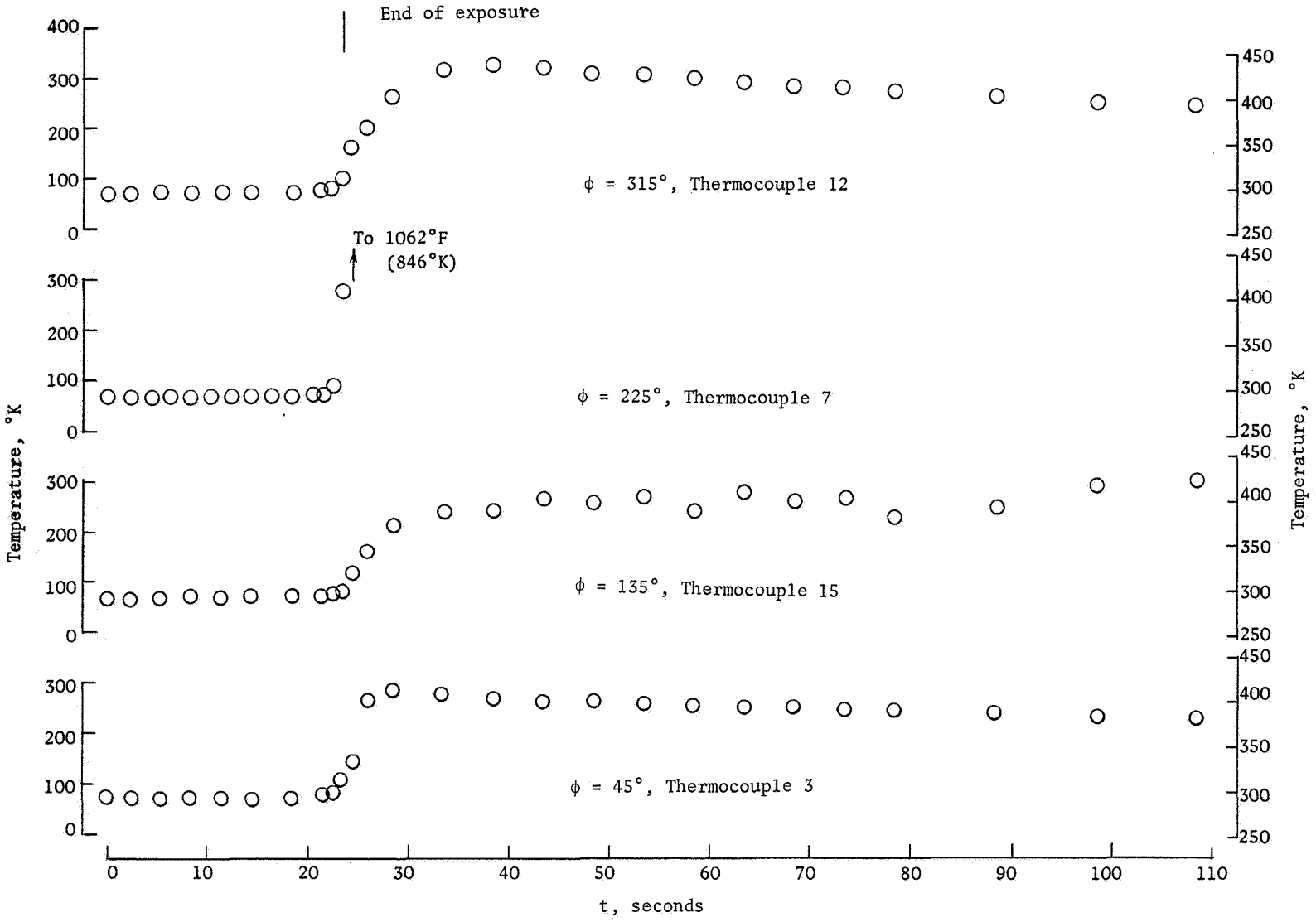

(c) Location s/r = 0.78.

Figure 13.- Continued.

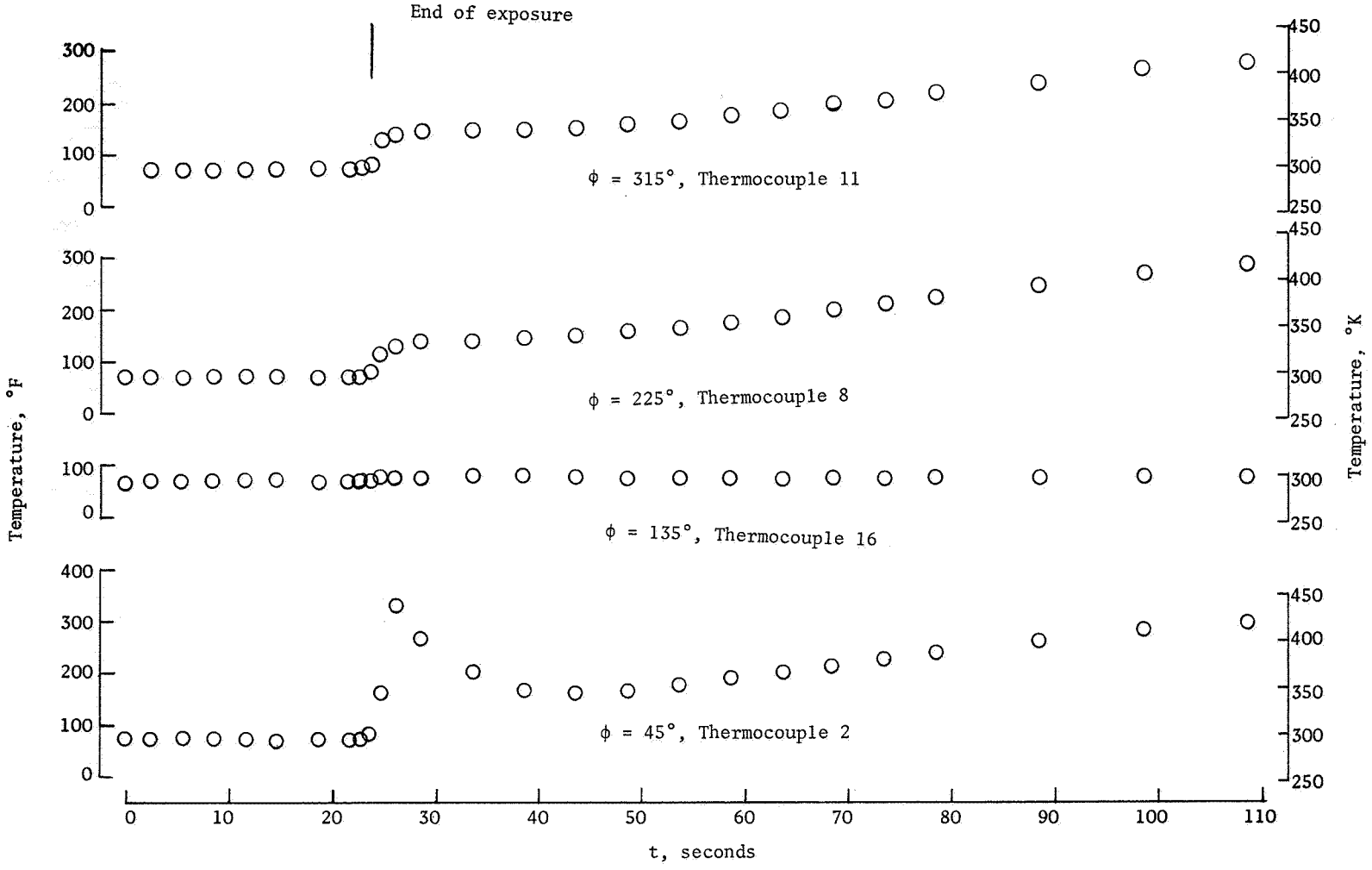

(d) Location s/r = 1.41.

Figure 13.- Continued.

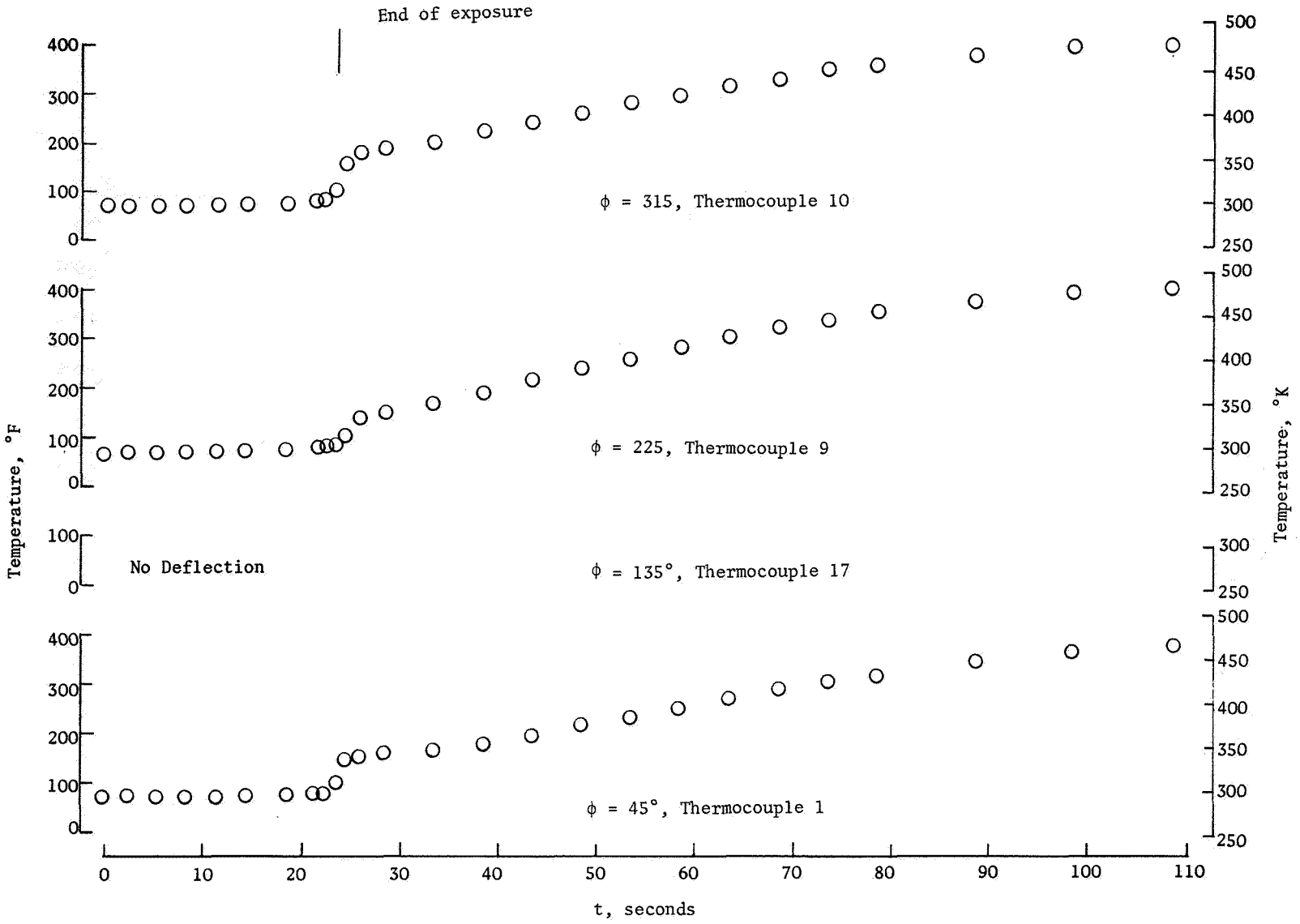

(e) Location s/r = 1.88.

Figure 13.- Continued.

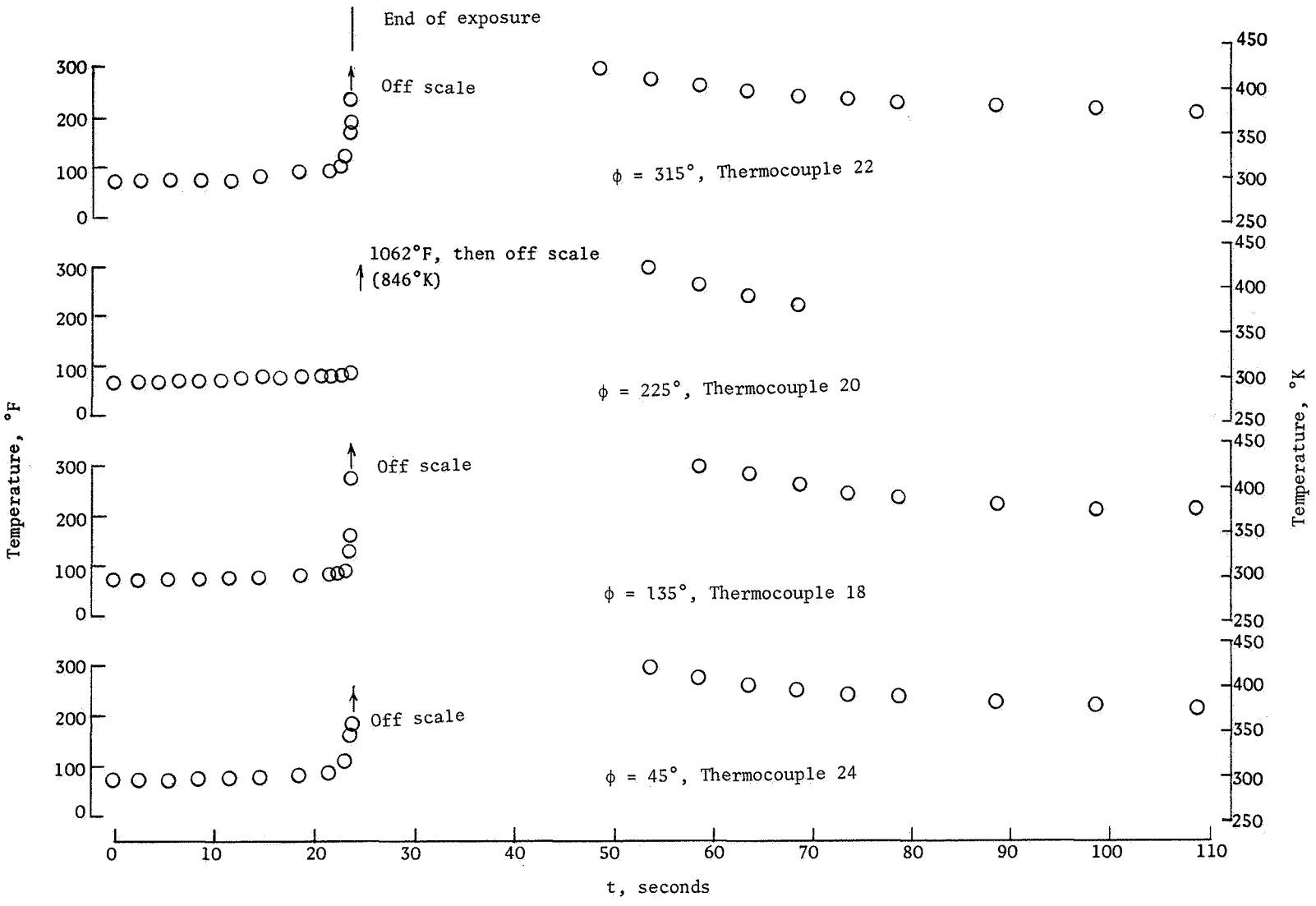

(f) Location s/r = 2.26.

Figure 13.- Continued.

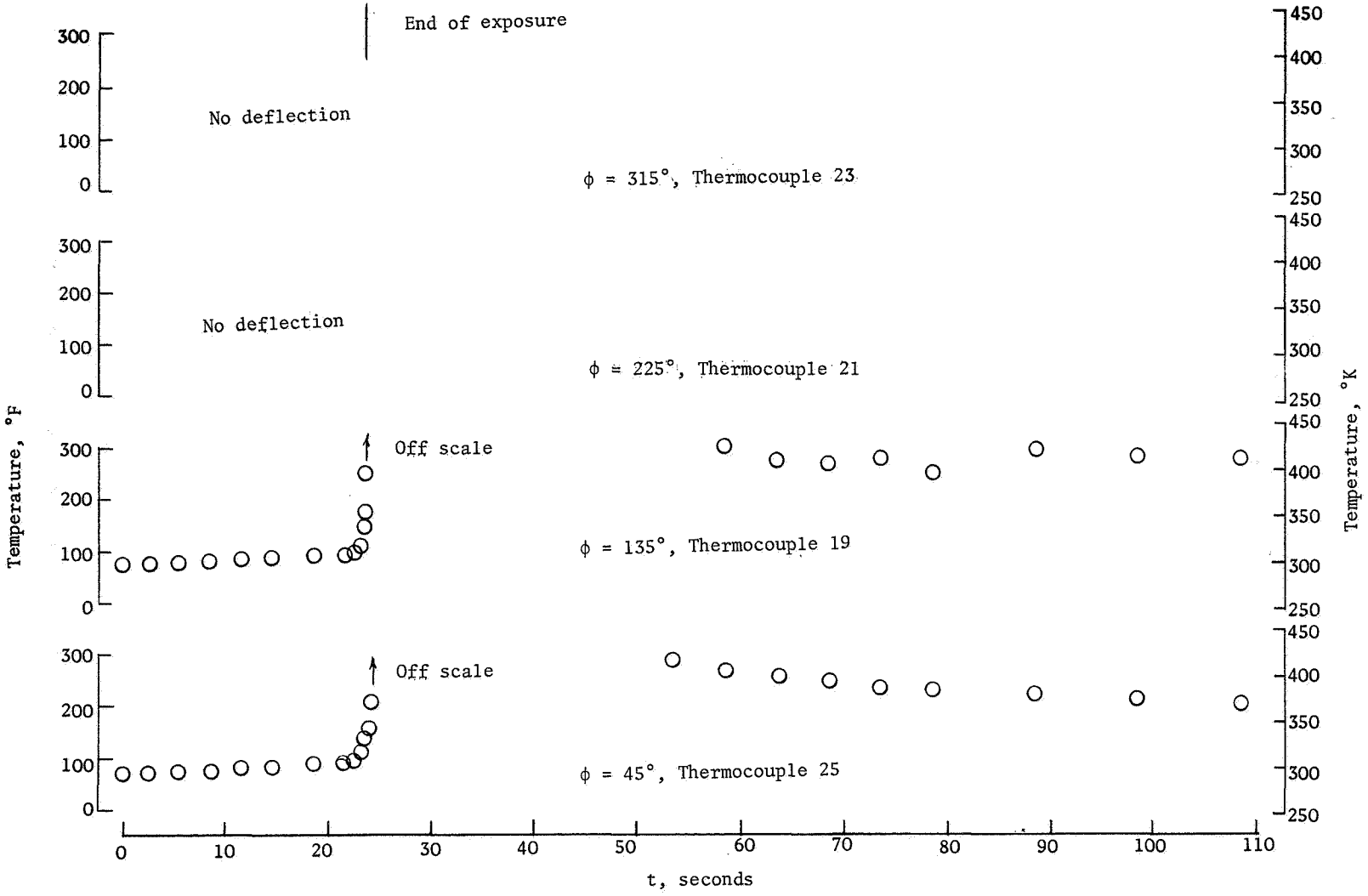

(g) Location s/r = 2.44.

Figure 13.- Concluded.

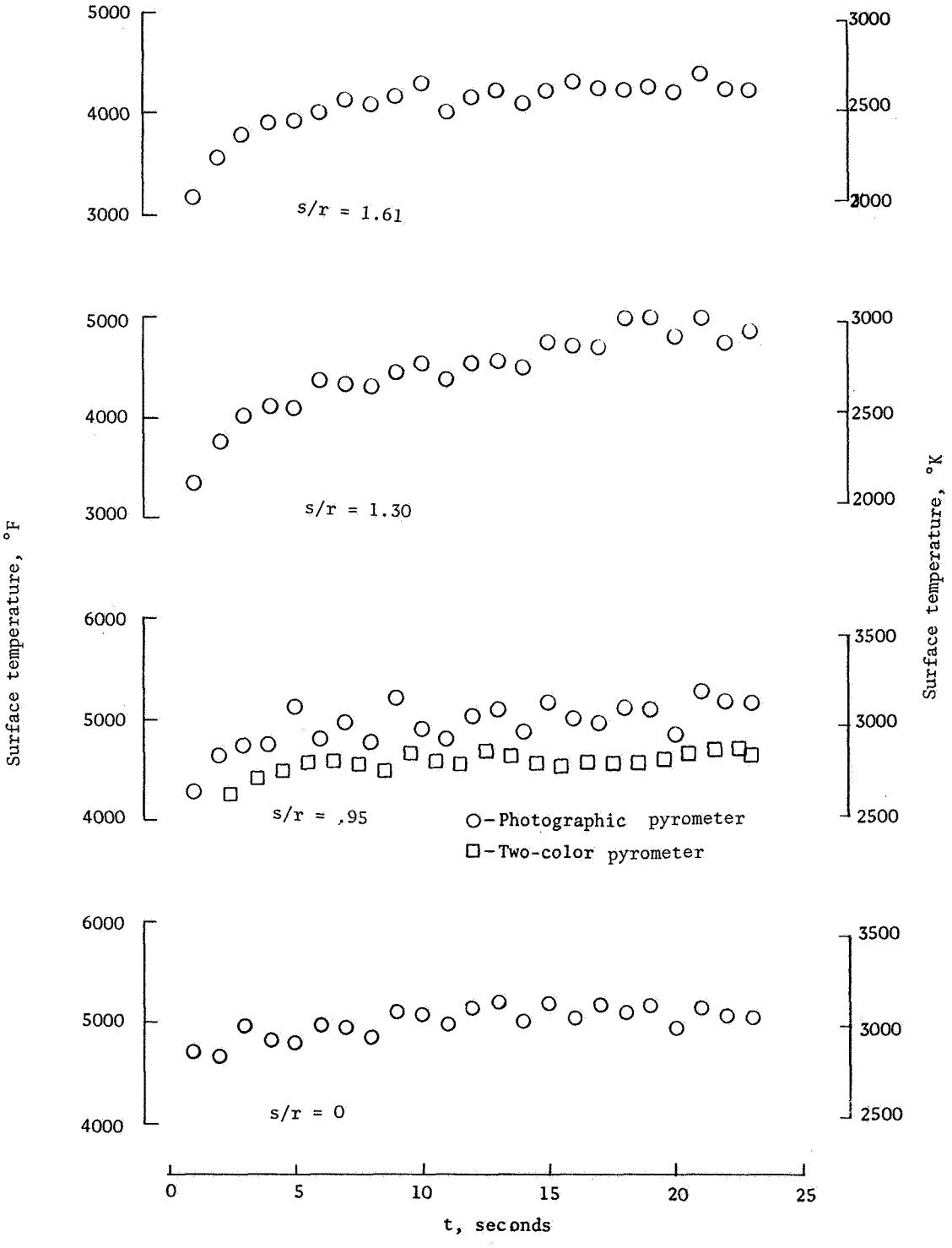

Figure 14.- Results of surface temperature measurements as a function of time.

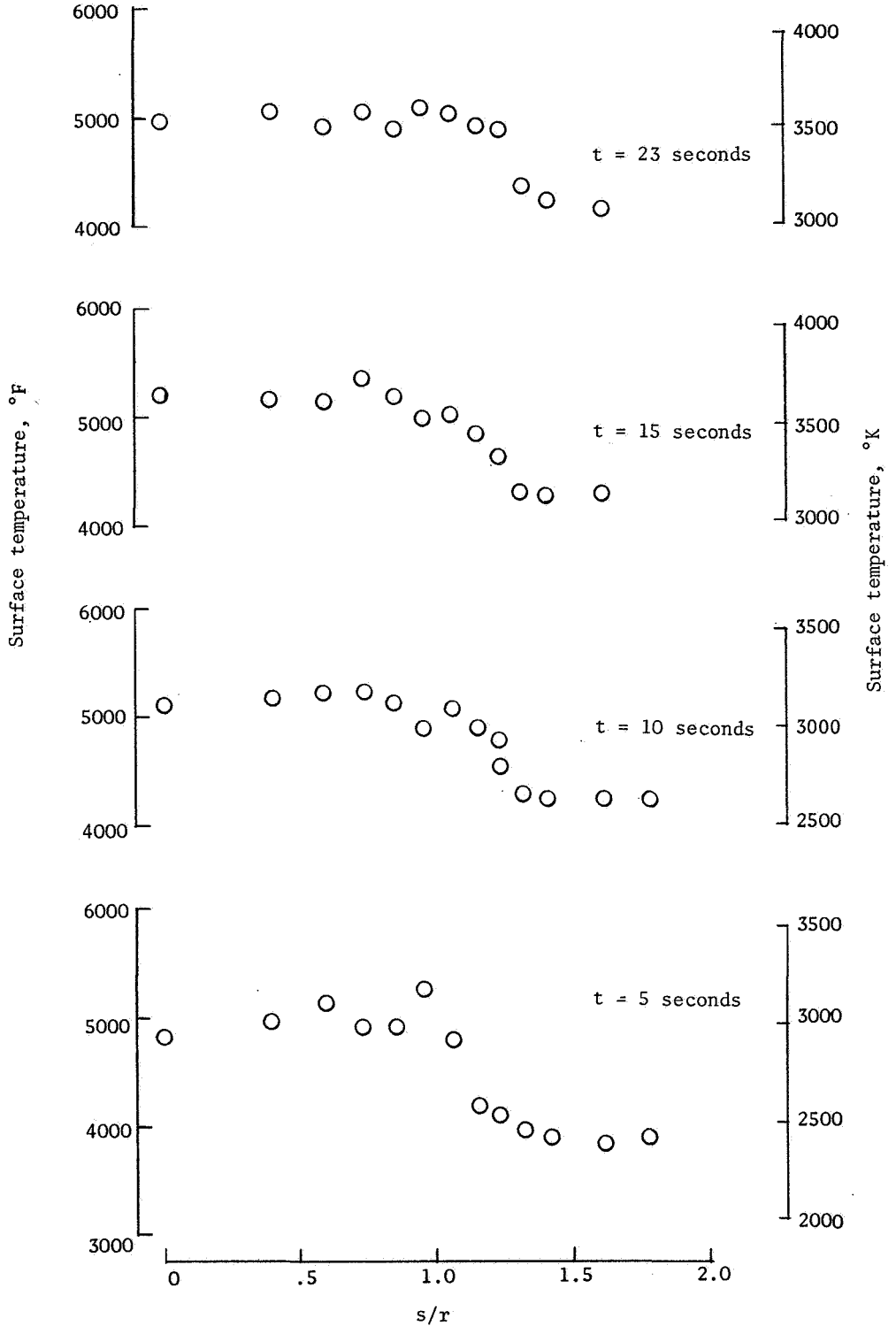

Figure 15.- Results of surface temperature measurements as a function of body location. Data from photographic pyrometer.

NATIONAL AERONAUTICS AND SPACE ADMINISTRATION
WASHINGTON, D.C. 20546

OFFICIAL BUSINESS

FIRST CLASS MAIL

POSTAGE AND FEES PAID
NATIONAL AERONAUTICS AND
SPACE ADMINISTRATION

POSTMASTER: If Undeliverable (Section 158
Postal Manual) Do Not Return

"The aeronautical and space activities of the United States shall be conducted so as to contribute . . . to the expansion of human knowledge of phenomena in the atmosphere and space. The Administration shall provide for the widest practicable and appropriate dissemination of information concerning its activities and the results thereof."

—NATIONAL AERONAUTICS AND SPACE ACT OF 1958

NASA SCIENTIFIC AND TECHNICAL PUBLICATIONS

TECHNICAL REPORTS: Scientific and technical information considered important, complete, and a lasting contribution to existing knowledge.

TECHNICAL NOTES: Information less broad in scope but nevertheless of importance as a contribution to existing knowledge.

TECHNICAL MEMORANDUMS: Information receiving limited distribution because of preliminary data, security classification, or other reasons.

CONTRACTOR REPORTS: Scientific and technical information generated under a NASA contract or grant and considered an important contribution to existing knowledge.

TECHNICAL TRANSLATIONS: Information published in a foreign language considered to merit NASA distribution in English.

SPECIAL PUBLICATIONS: Information derived from or of value to NASA activities. Publications include conference proceedings, monographs, data compilations, handbooks, sourcebooks, and special bibliographies.

TECHNOLOGY UTILIZATION PUBLICATIONS: Information on technology used by NASA that may be of particular interest in commercial and other non-aerospace applications. Publications include Tech Briefs, Technology Utilization Reports and Notes, and Technology Surveys.

Details on the availability of these publications may be obtained from:

SCIENTIFIC AND TECHNICAL INFORMATION DIVISION

NATIONAL AERONAUTICS AND SPACE ADMINISTRATION

Washington, D.C. 20546